Upregulation of phytoplankton carbon concentrating mechanisms during low CO_2 glacial periods and implications for the phytoplankton pCO_2 proxy

Heather M. Stoll[1*], Jose Guitian[1], Ivan Hernandez[1], Luz Maria Mejia[1] , Samuel Phelps[2], Pratigya Polissar[2], Yair Rosenthal[3] Hongrui Zhang[1], Patrizia Ziveri[4]

1. Department of Earth Sciences, ETH Zürich, Sonnegstrasse 5, 8092 Zürich, Switzerland
2. Biology and Paleo Environment, Lamont Doherty Earth Observatory, 61 Route 9W, Palisades, NY 10964, USA
3. Department of Marine and Coastal Sciences, Rutgers University,71 Dudley Road, New Brunswick, NJ 08901-8560, USA
4. Institute of Environmental Science and Technology, Universidad Autonoma de Barcelona, Bellaterra, Spain.

*To whom correspondence should be addressed: heather.stoll@erdw.ethz.ch

This is a post-peer-review, pre-copyedit version of an article published in Quaternary Science Reviews. The final authenticated version is available online at: https://doi.org/10.1016/j.quascirev.2019.01.012.

Stoll, H. M., Guitian, J., Hernandez-Almeida, I., Mejia, L. M., Phelps, S., Polissar, P., ... & Ziveri, P. (2019). Upregulation of phytoplankton carbon concentrating mechanisms during low CO2 glacial periods and implications for the phytoplankton pCO2 proxy. Quaternary Science Reviews, 208, 1-20

Abstract

Published alkenone ε_p records spanning known glacial pCO_2 cycles show considerably less variability than predicted by the diffusive model for cellular carbon acquisition and isotope fractionation. We suggest this pattern is consistent with a systematic cellular enhancement of the carbon supply to photosynthesis via carbon concentrating mechanisms under the case of carbon limitation during low pCO_2 glacial time periods, an effect also manifest under carbon limitation in experimental cultures of coccolithophores as well as diatoms. While the low-amplitude ε_p signal over glacial pCO_2 cycles has led some to question the reliability of ε_p for reconstructing long-term pCO_2, the $[CO_2]_{aq}$ in the tropical oceans during glacial pCO_2 minima represents the most extreme low CO_2 conditions likely experienced by phytoplankton in the Cenozoic, and the strongest upregulation of carbon concentrating mechanisms. Using a statistical multilinear regression model, we quantitatively parse out the factors (namely light, growth rate, and $[CO_2]_{aq}$), that contribute to variation in ε_p in alkenone-producing algae, which confirms a much smaller dependence of ε_p on $[CO_2]_{aq}$ in the low $[CO_2]_{aq}$ range, than inferred from the hyperbolic form of the diffusive model. Application of the new statistical model to two published tropical ε_p records spanning the late Neogene produces much more dynamic pCO_2 estimates than the conventional diffusive model and reveals a significant pCO_2 decline over the last 15 Ma, which is broadly consistent with recent results from boron isotopes of foraminifera. The stable isotopic fractionation between coccolith calcite and seawater dissolved inorganic carbon (here $\Delta_{coccolith\text{-}DIC}$) also shows systematic variations over glacial-interglacial cycles which may, following future experimental constraints, help estimate the degree of upregulation of parts of the algal carbon concentrating mechanism over glacial cycles.

1. Introduction

Photosynthesis by marine phytoplankton provides the base of the marine food web and fixes atmospheric CO_2 that is subsequently sequestered via the ocean's biological carbon pump. CO_2 is a key resource for phytoplankton photosynthesis, and algal physiology is sensitive to CO_2 availability. Consequently, there is growing interest in the impact of rising atmospheric CO_2 levels on the ecology of phytoplankton and higher trophic levels in the present and future oceans. At the same time, there is continued interest in using the sensitivity of marine algae to CO_2 in order to estimate atmospheric CO_2 during past time periods (Pagani, 2014). This latter objective has been pursued principally by measurement of the carbon isotopic fractionation during photosynthesis, denoted as ε_p, which is a marker for the supply of CO_2 to photosynthesis relative to the carbon demand of the cell. Carbon isotope fractionation during photosynthesis is predicted to be greatest when CO_2 availability is high relative to cellular carbon demand (Rau et al., 1996).

Quaternary glacial cycles, with interglacial maxima in pCO_2 around 280 μatm, and minima around 180 μatm (Petit et al., 1999), pose an apparent paradox in phytoplankton CO_2 acquisition. Theory predicts that the low glacial CO_2 should lead to a reduction in aqueous CO_2 (hereafter $[CO_2]_{aq}$) supply relative to cellular demand, and hence a reduced isotopic fractionation. However, most locations fail to show consistent ε_p minima during glacial periods (Andersen et al., 1999; Jasper et al., 1994; Palmer et al., 2010; Zhang et al., 2013). Different explanations have been evoked at different sites, but the most common explanations have been greater ocean to atmosphere CO_2 flux from upwelling of CO_2 rich water, or changes in nutrient supply affecting algal growth rate and carbon demand (Andersen et al., 1999; Jasper et al., 1994; Palmer et al., 2010).

Here, we review the available records and the potential factors contributing to fractionation over glacial cycles. We apply recent models for temperature sensitivity of phytoplankton growth rates in the ocean and assimilate a wide array of data from laboratory cultures of phytoplankton.

Models of carbon isotopic fractionation in phytoplankton were first compared with a very limited number of culture experiments in which CO_2, growth rate, or culture conditions were manipulated (Bidigare et al., 1997). Fortunately, a much larger experimental matrix of CO_2 and growth rates has subsequently been published (see compilation in Table 1).

This new analysis of culture and sediment data suggests that phytoplankton in the tropical oceans manifest a significant upregulation of carbon concentrating mechanisms (CCMs) to compensate for the low CO_2 during glacial periods. The energetic costs and trade-offs involved in such upregulation are unclear and warrant further study. The documentation of a systematic upregulation of CCMs during CO_2 minima suggests the potential for significant downregulation during future CO_2 increases, and indicates that this aspect of phytoplankton response is conserved across timescales from 10 generations in laboratory incubation experiments to 1x 10^8 generations over the last 300 ky. At the same time, the new analysis of culture studies leads us to develop a statistical multilinear regression model to quantitatively parse out the factors (namely light, growth rate, and $[CO_2]_{aq}$), that contribute to carbon isotope fractionation. We compare the implications of this alternative model with those of the diffusive model for pCO_2 estimates based on alkenone ε_p over the last 16 Ma.

2. Observed and expected phytoplankton isotopic fractionation over glacial cycles

2.1 Photosynthetic C isotopic fractionation via diffusive CO_2 uptake

The carbon isotopic fractionation by phytoplankton is classically described by a basic diffusive model to simulate the supply of CO_2 into the cell (via diffusion across the cell surface) relative to the demand by cellular growth (Francois et al., 1993; Goericke and Fry, 1994; Rau et al., 1996; Rau et al., 1997). This diffusive concept of CO_2 acquisition has formed the basis of nearly all prior applications of the phytoplankton pCO_2 proxy, with a few recent exceptions (Bolton et al., 2016; Heureux and Rickaby, 2015; Mejia et al., 2017) The governing equation defined by (Rau et al., 1996) is:

(1) $$\varepsilon_p = -\varepsilon_f + (\varepsilon_f - \varepsilon_d)\frac{\gamma \cdot \mu_i}{S \cdot c_e}\left(\frac{r}{D_T\left(1 + \frac{r}{r_k}\right)} + \frac{1}{P}\right)$$

Where ε_p is the fractionation between cellular organic matter and dissolved $[CO_2]_{aq}$ (c_e), ε_d is the fractionation factor due to diffusion (0.7 ‰ in water (Rau et al., 1996)) . ε_f is the maximum expressed fractionation during photosynthesis, here taken to be 25 ‰ following (Bidigare et al., 1997; Wilkes et al., 2017). γ is the cellular organic C quota, μ_i is the instantaneous cell growth rate accounting for differences in photoperiod, and S is the cellular surface area. The final term accounts for the processes at the cell boundary, including temperature-dependent diffusion rate of CO_2 (D_T), and the relative contribution to the CO_2 flux from extracellular conversion of HCO_3^- to CO_2 using r_k as the reacto-diffusive length. r is the cell radius of a sphere which would give an equivalent surface area, and P is the permeability or effective CO_2 transfer coefficient. Further description and standard units can be found in Rau et al., 1996.

In sediment samples for paleobarometry applications, ε_p is calculated as the isotopic difference between a measure of the $\delta^{13}C$ of algal biomass and the $\delta^{13}C$ of ambient aqueous CO_2. In most cases, the $\delta^{13}C$ of algal biomass is estimated using alkenone $\delta^{13}C$, which has been shown to be depleted relative to biomass by ~4.2 ‰ (Wilkes et al., 2018, Popp et al. 1998a). The carbon isotope ratio of DIC is estimated from coexisting planktic foraminfera, and the $\delta^{13}C$ of aqueous CO2 is determined using the temperature-dependent isotope partitioning between aqueous CO_2 and DIC.

In the equation, the product of cellular C quota and instantaneous growth rate is assumed to yield the C fixation rate. We incorporate the correction proposed by (Holtz et al., 2015) that the actual C fixation rate should be calculated as:

(2) $$C\ fixation\ rate = \gamma \cdot (e^{\mu} - 1)$$

This diffusive model predicts that ε_p should be largest when CO_2 supply is high, algal growth rates are low, and when algal cells are small and therefore have a high surface area to volume ratio, and that the relationship between ε_p and CO_2 should follow a hyperbolic form. Conversely, ε_p versus $1/CO_2$ should follow a linear form.

The approximation described in previous applications of ε_p for estimation of CO_2 (Jasper et al., 1994):

(3) $$\varepsilon p = \varepsilon f + \frac{b}{c_e}$$

was shown to be equivalent to the diffusive model, when:

(4) $$b = -(\varepsilon_f - \varepsilon_d)\frac{\gamma \cdot \mu_i}{S \cdot}\left(\frac{r}{D_T(1+\frac{r}{r_k})} + \frac{1}{P}\right)$$

This simplified formulation clarifies the dependence of *b* on variation in the cellular C content and surface area, which scale with cell size; as well as variation in the growth rate and the effective permeability to CO_2. When the effects of these factors are considered in aggregate, e.g. by empirical derivations of *b* from photic zone or culture samples, it must be remembered that the covariation and relative weight of each of these factors spatially in the modern ocean, or in culture experiments, may differ from past temporal significance and covariation of these factors. In practice, however, most previous work has interpreted variation in *b* to reflect either changes only in the growth rate parameter (Bidigare et al., 1997; Seki et al., 2010), or over long timescales also changes in the cell size and consequently in γ/S (Henderiks and Pagani, 2008; Seki et al., 2010). Potential variations in P have not been evaluated for glacial samples or the full range of published experiments with ε_p determinations in experimental culture, although some previous studies have acknowledged that the *b* term accounted for the degree of "leakiness" of cell uptake (Jasper et al., 1994).

2.2 Does phytoplankton isotopic fractionation over glacial cycles match the diffusive model?

Over Quaternary pCO_2 variations, ε_p has been estimated from alkenone $\delta^{13}C$ and estimation of surface ocean DIC from planktonic foraminifera, in the Central Equatorial Pacific (0.95°N, 138.96°W water depth 4287m) (Jasper et al 1994); the Western Arabian Sea (NIOP 464 22.15°N, 63.35°E; water depth 1470 m) (Palmer et al., 2010); the Western Tropical Atlantic (4°12.25N, 43°29.33W, 3042m water depth) (Zhang et al., 2013); and the Eastern subtropical South Atlantic in Angola Basin (GeoB 1016-3, 11.77°S, 11.68°W, 3410m water depth (Andersen et al., 1999)); map provided in Supplementary Figure S1. Given atmospheric pCO_2 variations from 180 to 287 ppm over the last 250

ka (Petit et al., 1999), surface ocean waters in equilibrium with the atmosphere would oscillate between 5 and 8 μM in these sites in the tropical ocean. The ε_p variations expected to accompany these variations in $[CO_2]_{aq}$ can be calculated according to the diffusive model, given estimation of the cell size, growth rate, and cell membrane permeability to CO_2.

The cell radius implied by the mean size of coccoliths from alkenone producing *Gephyrocapsa* in a global examination of surface sediments (Bollmann, 1997) is 1.81 μm according to regressions between coccolith size and cell size (Henderiks, 2008). We provide here some additional constraints on cell size for the Central Equatorial Pacific and Western Tropical Atlantic from new measurements of coccolith length, as described in the Supplementary Methods. We assign a phytoplankton growth rate using a recent model of coccolithophorid growth rate (Krumhardt et al., 2017) who estimates a maximum temperature-dependent growth rate modified by nutrient concentrations:

(5) $$\mu = \mu_{max} \cdot \left(\frac{N}{N + K_M}\right)$$

Where μ is nutrient limited growth rate (day^{-1}), μ_{max} is the maximum growth rate attainable at the growth temperature given by the power law of (Fielding, 2013), N is the concentration of limiting nutrient (in this case PO_4) and K_M is the half-saturation constant for growth limited by that nutrient, taken as 0.17 μM PO_4, following (Krumhardt et al., 2017). Light or trace nutrient limitation are not considered. Where NO_3 rather than PO_4 is the main limiting nutrient, this could be incorporated by using an estimated NO_3 concentration and constant for half-saturation of growth by NO_3.

For our estimations, the growth rate is driven in all cases by the temperature history reconstructed for each site, and an assumption about the PO_4 concentration. In the basic simulation, we assume constant PO_4 concentration, and only minor growth rate variations accompanying the slight glacial-interglacial temperature variations reconstructed for each site. For other estimates, variable PO_4 is evaluated; all parameters used in model ε_p determinations are given in Supplemental Table S1. Surface area is given by spherical geometry in the diffusive model, and cellular carbon quota is calculated using carbon–biovolume relationships (Popp et al., 1998b). A choice of P of 5.2

x10^{-5} m/s, within the range employed in sensitivity experiments of (Rau et al., 1997) of 1 x10^{-4} to 3 x10^{-5} m/s, produces the smallest average deviation between diffusive modeled ε_p and measured Holocene ε_p. Note that selection of a lower growth rate would require choice of a higher permeability (P) to minimize the difference between modeled and observed Holocene ε_p.

Using the same cell size, growth rate, surface area and permeability as for the Holocene, the diffusive model predicts ε_p which would be 5 to 5.4 ‰ lower (Equatorial Pacific, Arabian Sea, and Angola Basin) or 3.1 ‰ lower (Western Equatorial Atlantic) during glacial pCO_2 minima compared to interglacials (Figure 1; red squares). In contrast, measured ε_p during glacials at these sites is lower by only 0 to 2 ‰ (Figure 1; blue circles). The discrepancy between the diffusive model and the measured ε_p is significantly correlated with $[CO_2]_{aq}$ in three of the four sites examined, suggesting that the discrepancy is either due to factors which covary with CO_2 over glacial cycles, or that the diffusive model does not accurately simulate the dependence of ε_p on $[CO_2]_{aq}$. If the diffusive model of cellular carbon acquisition were accurate, then the much higher than predicted ε_p during glacial times would need to reflect either (a) cell sizes which were much smaller during glacial maxima, (b) cellular growth rates that were much lower during glacial maxima, or (c) tropical surface ocean with a greater sea-air CO_2 flux during glacials, elevating local $[CO_2]_{aq}$ above equilibrium with atmospheric concentrations. The tendency of predicted ε_p to be consistently higher than measured ε_p in the Western Equatorial Atlantic suggests that the contrast in growth rate among the sites, with higher growth rates in the other three sites, may be overestimated. Potentially the lower surface PO_4 in Western Equatorial Atlantic, driving lower modeled growth rates, is in reality partially compensated by lower light attenuation and less light limitation of growth compared to more productive higher PO_4 sites. Light limitation is not incorporated in the Krumhardt et al. (2017) growth rate model.

Smaller cell radius increases the surface area to volume of spherical cells such as coccolithophorids. In the diffusive model, a factor of two decrease in the mean cell radius would be required to explain the elevated glacial ε_p by this mechanism alone. However, our new observations

of coccolith length suggest similar length and thus similar cell sizes for the Western Tropical Atlantic, and slightly larger coccolith size in the last glacial maximum in the Equatorial Pacific. Consequently, cell size is unable to explain the deviation between predicted and observed ε_p between interglacial and glacial times (Figure 1A and B, green triangles). In addition, the nearly twofold increase in average mass of coccoliths from alkenone producing *Gephyrocapsa* and *Emiliania huxleyi* in tropical regions during the last glacial maximum (Beaufort et al., 2011) reflects either larger average coccolithophores cell size and/or thicker coccoliths. If cell size were smaller by a factor of two, then the twofold increase in coccolith mass determinations would require a nearly fourfold increase in coccolith thickness (mass/area) equivalent to the entire range among diverse extant strains of Noëlaerhabdaceae determined in culture (Bolton et al., 2016). Together, these observations suggest alkenone-producing coccolithophorids were not smaller during the LGM, requiring an alternative explanation for the damped ε_p response.

Lower growth rates reduce the cellular carbon demand, and could in theory compensate for a reduction in diffusive carbon supply due to low glacial pCO_2. Existing models for the temperature dependence of coccolithophorid growth rates (Krumhardt et al., 2017) suggest that the 1-3 degree cooler glacial temperatures in the tropics would depress growth rates only slightly, leading to only a small effect on the ε_p modeled for glacial times (Supplementary Table S1, effect incorporated in red symbols in Figure 1). $[CO_2]_{aq}$ is not growth-limiting until much lower concentrations, with a half saturation constant for *E. huxleyi* of 1.7 μM (Feng et al., 2017). Large decreases in nutrient supply would be an alternative mechanism to depress growth rates during the glacial. Few proxies exist for surface ocean nutrient concentrations. However, proxies interpreted to reflect upper photic zone productivity suggest that nutrient supply changes were either of insufficient scope and/or inappropriate timing to account for the stability in measured ε_p (Figure 1 purple crosses; growth rate proxies shown in Supplemental Figure S2). Estimations of the magnitude of possible changes in growth rate are best constrained for the Equatorial Pacific and Western Tropical Atlantic, because for these sites, estimations of the relative abundance of deep photic coccolithophorid species

Florosphaera profunda have been made ((Beaufort, 2007) and new counts here for Western Tropical Atlantic). A regression between *F. profunda* abundance and global PO_4 (Hernandez-Almeida, 2018) allows estimation of PO_4, from which growth rate variations can be estimated (Krumhardt et al., 2017). Despite the large range in growth rate suggested for both sites, the timing of changes in growth rate is not coincident with the glacial-interglacial 100 ky variations in $[CO_2]_{aq}$, and therefore inclusion of these growth rate variations in estimation of ε_p using the diffusive model does not improve agreement with measured ε_p (Figure 1A, B). In the Arabian Sea and Angola Basin, proxies for changes in relative growth rate from Cd/Ca ratios in planktic foraminifera (Palmer et al., 2010) and nitrogen isotopes in organic matter (Holmes et al., 1997), respectively, can be used to evaluate the timing of likely changes in growth rate. However, even when these changes in growth are assumed to correspond to variations of 50% around modern PO_4 concentrations, their timing is not well matched to improve the fit between expected and observed ε_p (purple crosses, Figure 1 C, D). Overall, inferred changes in nutrient supply are not suitably timed to cause lower glacial growth rates and therefore do not improve the discrepancy between observed and expected ε_p values.

Previous studies have interpreted the higher than expected glacial ε_p as indicating that the measured sites were greater sources of CO_2 to the atmosphere during the glacial times than present (Andersen et al., 1999; Jasper et al., 1994; Palmer et al., 2010). Upwelling of deep water enriched in CO_2 from respiration can locally elevate $[CO_2]_{aq}$ and pCO_2 with respect to the atmosphere. However, upwelling of this deep water also entails upwelling of major and trace nutrients elevated by respiration of organic matter. Consequently, at the same time that higher $[CO_2]_{aq}$ should promote a higher ε_p, the stimulation of growth rates by higher nutrient supply, would promote lower ε_p. Indeed, modern photic zone alkenone samples suggest a low sensitivity of ε_p to air-sea disequilibrium due to the counteracting effect between nutrient and $[CO_2]_{aq}$ (Mejia et al., 2017). In the modern photic zone, tropical sites such as those with glacial-interglacial records (T > 23 °C) show no statistically significant change in ε_p with increasing measured $[CO_2]_{aq}$ nor increasing degree of sea-air

CO_2 outgassing (Figure 2). Consequently, we consider significantly increased sea-air disequilibrium in all tropical locations during glacial cycles an unlikely explanation for the consistent difference between predicted and observed ε_p values over glacial cycles.

3. Evaluating deviation from the diffusive model

3.1 Quantifying deviation from the diffusive model in phytoplankton ε_p

To investigate the potential causes of the unexpected ε_p stability over glacial-interglacial cycles, we make a simple estimation of the degree to which the measured ε_p deviates from the diffusive model. Since the principal undefined term from Equation 1 is the permeability (P) of the membrane, here we vary the P parameter, rather than using a constant value as assumed in previous applications. As Figure 3 shows, no single permeability value is able to match all of the data from glacial-interglacial cycles. Likewise, no single permeability value is able to fit all existing culture experiments, for which uncertainties in the other physiological parameters of the model are minimal (Figure 3).

Calculating a variable P is equivalent to estimating by how much the diffusive curve must shift to match the ε_p of each sample. One can estimate the P as a variable, solving for:

(6) $$P_{var} = \frac{\varepsilon_f - \varepsilon_d}{\varepsilon_f - \varepsilon_p} \cdot \frac{\gamma \cdot (e^{\mu} - 1)}{c_e \cdot S}$$

Using our previous assumptions regarding growth rates and cell sizes of alkenone producers at the four sites in question, Figure 4A shows the estimated P variations for samples spanning the Quaternary glacial cycles. We compare these with the equivalent variations in P calculated for culture experiments (Figure 4B). These cultures represent the most fully constrained conditions, where growth rate, cell size, and $[CO_2]_{aq}$ are all independently determined, and therefore represent the most precise quantification of the degree of deviation from the diffusive model. In both the sediment and culture samples, there is a large range in estimated permeability. To explain the ε_p variations observed in late Quaternary sediments, for the estimated growth rates, a threefold

permeability variation, from $3x10^{-5}$ to $1x10^{-4}$ m/s, is required. Culture experiments would require over a hundredfold increase (from $3.4x10^{-6}$ to $3.7x10^{-4}$ m/s) in CO_2 permeability as the CO_2 supply declines. In the culture dataset, the P_{var} is most strongly correlated to $\ln([CO_2]_{aq})$ and instantaneous growth rate, moderately correlated to culture conditions which promote higher growth such as light, and negligibly correlated with temperature (Supplemental Table S2). Despite uncertainty in absolute growth rates in sediment ε_p records, the similarity in P variation over glacial/interglacial cycles and in cultured coccolithophorids suggests that the deviation from diffusive behavior, estimated via a variable permeability, is a systematic response by phytoplankton to CO_2 and growth rate. This therefore represents a ubiquitous physiological response, whether over the timescale of several weeks in the laboratory or over 10^8 generation periods of the last 300 ky.

3.2 Do phytoplankton accomplish such a dynamic range in permeability?

The question of whether phytoplankton are capable of accomplishing a variation in cell CO_2 permeability over three orders of magnitude under different conditions remains unclear. Different biomembranes can have widely different CO_2 permeabilities depending on their function (Endeward et al., 2014). Higher CO_2 permeability can be achieved either by decreasing sterol (e.g. stigmasterol and cholesterol) content and/or by incorporating protein channels (e.g. aquaporins and Rhesus proteins)(Endeward et al., 2014; Kai and Kaldenhoff, 2014). Different ranges of permeability variation have been reported in different studies. For instance, experimental studies with pH microelectrodes to study steady state permeability in synthetic lipid bilayers show that insertion of aquaporin NtAQP1 does not further increase CO_2 membrane permeability, and that increasing cholesterol from 0 to 67% resulted in a 6-fold decrease in CO_2 permeability of the synthetic bilayer (Kai and Kaldenhoff, 2014). The scope of permeability change of this study contrasts with previous results when enriching and depleting the cholesterol of human red kidney membranes and synthetic lipid bilayers, detecting a 3 orders of magnitude change in CO_2 permeability using Membrane Inlet Mass Spectrometry (MIMS) (Itel et al., 2012).

The typical cholesterol composition of most eukaryotic biomembranes is ~40% cholesterol, which entails a CO_2 permeability of 1 x10^{-4} m/s (Itel et al., 2012). Since biomembranes can be enriched in cholesterol up to 77% (Endeward et al., 2014), in principle, it would be possible for phytoplankton cells to dramatically regulate their cholesterol content to achieve substantially higher or lower CO_2 permeabilities. However, a significant decrease in cholesterol composition would reduce their mechanical stability and the barrier function to other undesired molecules. Moreover, direct estimates of cell membrane permeability via MIMS have been made for four species of diatoms, and their range is much more constant, varying only between 1.3 (+/- 0.2) to 6.7 (+/-1.1) x 10^{-4} m/s (Hopkinson et al., 2011) (Figure 4). It remains to be determined whether the physiological capabilities of modulating membrane CO_2 permeability are greater in coccolithophorids than those observed for diatoms.

In contrast to the relatively small range of directly measured diatom permeabilities among species, the range of carbon isotopic fractionation (ε_p) of cultured diatoms, similar to that of coccolithophorids, implies a larger range in the calculated P value in order to match the ε_p predicted by diffusive model. Measured values of ε_p in the cultured pennate diatom *P. tricornutum* (Riebesell et al., 2000a) require P variation from 2 x 10^{-6} m/s to 2 x 10^{-4} m/s (Figure 5). This P variability is far greater than the range observed among different diatom species of different sizes and surface area/volume ratio. Therefore, there must be a factor, instead or in addition to permeability modulation, that explains ε_p variations in diatoms and other phytoplankton groups.

In the case of the diatom *P. tricornutum*, ε_p is known to not be regulated by a single cell passive diffusion model, but rather by a "chloroplast pump" system which elevates CO_2 within a small compartment at the site of photosynthesis (i.e. pyrenoid; Figure 5) (Hopkinson, 2014; Hopkinson et al., 2011). In this diatom, carbon concentration at the pyrenoid, within the chloroplast, of up to tenfold, is accomplished by (a) generating a downgradient CO_2 influx across the plasma membrane by b) catalyzing a hydration of CO_2 to HCO_3^- in the cytosol or chloroplast envelope, and

pumping HCO_3^- successively up gradient into the chloroplast and pyrenoid, followed by (c) dehydration of HCO_3^- to CO_2 in the pyrenoid. The effects on ε_p in diatoms have been simulated in several two-compartment carbon-isotope mass balance models (Cassar et al., 2006; Hopkinson et al., 2011; Schulz et al., 2007). Under the assumption of constant cell membrane CO_2 permeability as measured by MIMS, the carbon isotopic two-compartment model (Hopkinson et al., 2011) has been applied in an inverse fashion to the same *P. tricornutum* culture data to diagnose the potential significance of HCO_3^- transport to the chloroplast (Mejia et al., 2017). When the variability of P (P_{var}) is calculated for these cultures using Equation 5, it correlates linearly with the inferred significance of active transport of HCO_3^- to the chloroplast (evaluated as the ratio of HCO_3^-transport to the chloroplast relative to carbon fixation). The detailed understanding of the carbon concentrating mechanism (CCM) in *P. tricornutum* suggests that while estimation of P_{var} provides a reproducible and independent first order quantification of the relative degree of deviation of ε_p from the diffusive model, it is likely not a realistic representation of the actual physical process responsible for the variation in fractionation, neither in diatoms nor in other phytoplankton. We suggest, instead, that ε_p in coccolithophores, like diatoms, is strongly influenced by carbon concentrating mechanisms. This is further supported by results from field diatom isotope labeling studies, in which CO_2 enrichments of 2 to 7-fold at the site of photosynthesis have been inferred (Kranz et al., 2015).

Active carbon concentrating mechanisms to enhance the concentration of CO_2 at the site of photosynthetic carbon fixation have been documented for a wide range of phytoplankton, from cyanobacteria, diatoms, and green algae. Supplementary mechanisms of concentrating carbon at the active site of the photosynthetic enzyme RuBisCO contribute significantly to the observed photosynthetic rates in most eukaryotic phytoplankton because the RuBisCO enzyme is inefficient under current low levels of CO_2 in seawater (Raven et al., 2014; Reinfelder, 2010). Components ubiquitous to CCMs of all aquatic oxygenic photosynthesis include: (a) a microcompartment in which CO_2 is enriched at the site of RuBisCO, and which helps to minimize CO_2 leakage, (b) inorganic carbon transporters which require energy either directly or to establish an ion gradient, (c) carbonic

anhydrases (CA) to accelerate interconversion between CO_2 and HCO_3^-, (d) proton pumps to maintain homeostasis following dehydration of HCO_3^- (Meyer and Griffiths, 2013).

The combination of MIMS experiments and genetic manipulation conducted to provide a detailed model of architecture of the diatom CCM has not yet been conducted for coccolithophores. Some molecular components associated with the CCM in other eukaryotic algae, including CA and HCO_3^- transporters, are recognized in the *E. huxleyi* gene sequence (Meyer and Griffiths, 2013). However, the location of CA is not experimentally confirmed and the cell membrane CO_2 permeability of coccolithophorids has not been experimentally determined. Furthermore, even within the same strain and experimental conditions in the same laboratory, different techniques give widely different estimates on the significance of direct HCO_3^- transport across the cell membrane. ^{14}C disequilibrium methods suggest it is only employed at very low CO_2 (Kottmeier et al., 2014), as in *Chlamydomonas* (Wang et al., 2015). However, MIMS analyses suggest HCO_3^- uptake is significant across a range of low to modest CO_2 concentrations (Kottmeier et al., 2016). Initial proteomics on *E. huxleyi* showed no significant differences in cells acclimated to high or low CO_2 (Jones et al., 2013). Consequently, multiple divergent models accounting for three cellular compartments (cytosol, chloroplast, and coccolith vesicle) and the calcification process have been developed for coccolithophorids (Bolton and Stoll, 2013; Holtz et al., 2017; McClelland et al., 2017). However, because such models are currently experimentally under-constrained, they feature very divergent assumptions, which lead to different inferences about the CCM and mechanisms for isotopic fractionation in organic matter.

Until a consensus, experimentally supported CCM model for coccolithophorids is developed, the assessment of the variability in permeability P_{var} may serve as an empirical index of CCM significance in coccolithophorids which is reproducible and not dependent on the assumptions of any particular model of the intracellular coccolithophorid carbon concentrating system. The concept of elevated whole cell permeability allowing greater than expected cycling of carbon through the cell, is analogous to the internal CCM producing a higher than expected rate of cycling of carbon through

the specific site of the photosynthetic system. Both a hypothetical increase in P_{var} and actual CCM upregulation allow carbon acquisition at the site of photosynthesis to be leakier than expected for low CO_2 concentrations. Further studies are required to determine whether coccolithophorids' plasma membrane permeability is similar to other marine phytoplankton and whether it is variable in response to CO_2 or other environmental factors such as temperature.

Our inferences from the available data on isotopic fractionation in coccolithophorid biomarkers from the tropical oceans and calculation of P_{var} suggest that coccolithophorids significantly upregulate the CCM to compensate for the low $[CO_2]_{aq}$ concentrations characteristic of glacial maxima. It is also possible that coccolithophorids significantly regulate membrane permeability to compensate for the low $[CO_2]_{aq}$. The tropical oceans feature the lowest $[CO_2]_{aq}$ concentration of the global ocean, and experience the greatest degree of carbon limitation of photosynthesis during glacial maxima, with concentrations as low as 5 μM. In laboratory cultures under optimal nutrient, light, and temperature conditions, phytoplankton upregulate CCM. These results suggest that despite resource limitations in the ocean, significant energy is nonetheless invested in CCM upregulation during glacial times.

The overview of both glacial and culture data has implications for interpretation of ε_p variations in sediments on longer timescales as well. The culture and recent sediment data show that ε_p does not exhibit a hyperbolic relationship with CO_2 as expected by the diffusive model, but rather that the operation of CCM leads to a much more linear or power relationship between ε_p and CO_2. Therefore, in the subsequent section we review the empirical relationships between ε_p, CO_2 and other parameters suggested by culture data and their implications for interpreting ε_p variations in coccolithophorids.

4. Empirical relationships between ε_p, CO_2 and key drivers of fractionation in cultured coccolithophorids

To better understand the implications of non-diffusive CO_2 supply on photosynthetic fractionation and the interpretation of past ε_p records, we evaluate empirically the parameters that best predict ε_p in the published culture experiments (compiled in Table 1). In these experiments, $[CO_2]_{aq}$ variations in the range of 0 to 30 μM are accomplished by both pH and DIC manipulations as well as bubbling culture media with gas mixtures of varying pCO_2. All experiments with $[CO_2]_{aq}$ above 30 μM were achieved through elevating seawater DIC well above modern concentrations, with the exception of one experiment produced by CO_2 bubbling which attained a concentration of 274 μM (Bidigare et al., 1997).

We have sought regressions with parameters expected to be significant based on previous discussions of fractionation (CO_2, cell radius, growth rate, and light). Variations in fractionation between 24 hour illumination and 16 hour/8 hour light/dark cycles has been described (Rost et al., 2002), but 24 hour illumination is not expected at any of the sites where ε_p has been estimated from marine sediments so this variable has not been explored independently; rather the photoperiod is incorporated into the calculation of the instantaneous growth rate. Data were not sufficiently complete to evaluate the relationship between the photosynthetic and calcification processes due to the absence of PIC/cell or PIC/POC in most studies. The variables $[CO_2]_{aq}$ and light were natural log transformed prior to regression analysis, as unimodal data is superior in regression models.

4.1 Statistical model for ε_p dependence on CO_2 from culture data

One persistent challenge in attributing variation in ε_p to different physiological and forcing parameters, both in culture studies and natural populations, is the covariation of multiple factors. For example, in the full culture dataset, CO_2 and DIC are highly correlated, and light and growth rate are moderately correlated (Supplementary Figure S3). To address the covariation of CO_2 and DIC, we conduct regression analysis using the full dataset, and then using the subset of the cultures which

were grown in a narrower range of DIC, from 1.6 to 3 mM, a range that more closely approximates the DIC concentrations in the modern and glacial oceans. To address the covariation of growth rate and light, we complete regressions with only growth rate, document the residual correlation with light, and compare with the full regression including both light and growth rate.

In the full dataset, a strong prediction of ε_p can be made using ln ($[CO_2]_{aq}$), ln (light intensity), instantaneous growth rate, and radius (Table 2a; r^2=0.68). In this regression, CO_2 and light have positive coefficients (that is, have positive covariation with ε_p), whereas growthrate and radius have negative coefficients (varying inversely with ε_p). The positive covariation between ε_p and CO_2, and the inverse dependence between ε_p and growth rate and radius, follow general expectations that higher CO_2 supply permits greater expression of the kinetic fractionation by RuBisCO, and that larger, and faster growing cells, have reduced selectivity. Biological modulation of cellular carbon uptake and internal carbon allocation, however, modulate the form and slope of these relationships. The four parameters are all highly significant and have broadly similar impacts on ε_p given the range of variation across the culture dataset. In the full dataset, a comparably strong prediction of ε_p (r^2=0.7) can be made using DIC as an independent parameter in addition to $[CO_2]_{aq}$ (Table 2b). In this dataset, the coefficients of light, growth rate, and radius are similar, but the coefficient of CO_2 is significantly higher (2.38 vs 1.45) and the coefficient of DIC is negative, implying that elevated DIC leads to lower ε_p.

4.1.1 Effect of DIC

In a regression model limited to culture data with DIC in the range of 1.6 to 3, the coefficient of CO_2 is higher (2.66) than either of the preceding regression models and the strength of the prediction is comparable (r^2 = 0.70) (Table 2c). This supports the inference of the previous model: high DIC lowers ε_p and artificially depressed the dependence of ε_p on CO_2 in the full dataset.

If there is direct uptake of HCO_3^- across the cell membrane, and the degree of uptake is proportional to the concentration of HCO_3^- and DIC in the growth media, as suggested by some

cellular models (Holtz et al., 2015, 2017), then the media DIC concentration may affect ε_p. Because HCO_3^- in seawater has a higher $\delta^{13}C$ than CO_2, significant cellular uptake of HCO_3^- could increase the $\delta^{13}C$ of the source of C to the cell, increasing $\delta^{13}C$ and POC and lowering ε_p compared to when the cell is supplied by CO_2 alone (Keller and Morel, 1999). To date, there is uncertainty from experimental data regarding the significance of active HCO_3^- uptake across the cell membrane, and if there is significant active HCO_3^- across the cell membrane, whether it is more dependent on the degree of cellular C limitation and upregulation of the HCO_3^- transport system, or on the HCO_3^- gradient between the external seawater and the cell, in which case seawater DIC is significant. ^{14}C disequilibrium methods suggest it is only employed at very low CO_2 (Kottmeier et al., 2014), as in *Chlamydomonas* (Wang et al., 2015), and that CO_2 dominantly enters the cell as CO_2, potentially subject to hydration to HCO_3^- within the cell, as observed in diatom *P. tricornutum* (Hopkinson, 2014). On the other hand, MIMS analyses suggest HCO_3^- uptake in coccolithophores is significant across a range of low to modest CO_2 concentrations (Kottmeier et al., 2016). If the significance of HCO_3^- uptake depends primarily on cellular demand, and is elevated at low $[CO_2]_{aq}$, this would be expected to depress ε_p at low $[CO_2]_{aq}$, steepening the gradient between ε_p and $[CO_2]_{aq}$. In contrast, if HCO_3^- uptake were dominantly constitutive, rather than upregulated, and dependent on the HCO_3^- and DIC in the growth media, then greater HCO_3^- uptake in cultures of high DIC, here strongly positively correlated with $[CO_2]_{aq}$ in the full dataset, would lead to a reduced gradient between ε_p and $[CO_2]_{aq}$. A combined scenario in which HCO_3^-uptake across the cell membrane is upregulated below some threshold of CO_2 limitation, but the actual HCO_3^-- flux is dependent on the HCO_3^- concentration, is possible but its consequences for ε_p would depend strongly on the channel half-saturation constant (Holtz et al., 2017). Confirming and constraining well this DIC effect will require culture experiments at comparable $[CO_2]_{aq}$ that maintain a DIC concentration in the range of 2-3 mM in parallel with those that feature modified DIC. Also, the physiological consequences of DIC concentrations well outside the modern realm should be evaluated, since in some experiments,

extreme elevation of DIC was correlated with a threefold reduction of growth rates (McClelland et al., 2017).

4.1.2 Effect of light in cultures and the water column

The influence of light emerges as an important control with a positive coefficient, meaning high light correlates with higher ε_p. However, light correlates modestly with growth rate (Supplemental Figure S3). Without including light as a predictive variable, the residuals from the predictive model (prediction-observation) correlate modestly but significantly with light (r^2=0.48; p value <0.001). This can be seen in comparisons of predicted vs observed ε_p in regression models which incorporate or exclude light (Supplemental Figure S4) as a systematic contrasting offset of high and low light experiments from the 1:1 line between prediction and observation when light is not included in the model.

An effect of light on fractionation has been noted and discussed previously (Cassar et al., 2006; Hoins et al., 2016; Holtz et al., 2017; Riebesell et al., 2000a; Rost et al., 2002; Tchernov et al., 2014). To first order, the effect of light represents changes in either leakage or the inorganic carbon source (Rost et al., 2002). Riebesell et al (2000) suggested that ATP and NADPH must be delivered in a ratio (ATP/e-) matched to the needs for biomass synthesis, and that a greater proportion of non-linear to linear electron transport increases the ATP/e- ratio and thus the amount of chemical energy available for processes such as active carbon transport. Higher light conditions provide a higher ATP/e- ratio and greater energy available for active carbon transport (Cassar et al., 2006). Potentially, high light stimulates massive carbon cycling, a light-dependent influx and efflux of inorganic carbon independent from carbon fixation (Tchernov et al., 2014).

The significance of light on ε_p implied by this regression model is large (e.g. Figure 6A), especially compared to the sensitivity of ε_p on $[CO_2]_{aq}$ (Figure 6B); ε_p increases 4 to 10 ‰ over the light range from 10 to 250 $\mu Em^{-2}s^{-1}$, as highlighted in previous experiments (Rost et al., 2002). Through much of the mid and low-latitude tropical oceans, the incoming irradiance at the ocean

surface is high and varies little. However, very large variations in photosynthetically active radiation (PAR) are encountered with depth in the ocean photic zone, with attenuation modulated strongly by chlorophyll concentration. Consequently, the entire experimental range in light values in cultures may be encountered vertically in the photic zone at any one location (Figure 7A). Using the slope of the regression equation provided in Table 2c, a dramatic decrease in ε_p with increasing depth is predicted (Figure 7C). The limited data on alkenone ε_p from the Pacific gyre (Tolosa et al., 2008) do suggest a decrease in ε_p with depth in the central gyre location (Figure 7C) compared to the surface. However, the observed decrease in ε_p with depth is much smaller than predicted by light attenuation alone (Figure 7C), likely because the growth rate is also reduced due to light limitation with depth. The degree of dependence of growth rate on irradiance determines whether there is a net increase or decrease in ε_p predicted with depth. A modest, rather than strong, dependence of growth rate on irradiance, coupled with a direct dependence of ε_p on light, yields a curve that matches the scale of the ε_p decline with depth in the central gyre setting (Figure 7C). Two factors may contribute to the predominance of this lower apparent growth rate dependence on irradiance. First, photoadaptation, including modulation of cellular chlorophyll content, may help cells maintain higher growth rates in darker settings. In some settings, the lower apparent growth rate dependence on irradiance may reflect the net effect of both nutrients and light on growth, where scarcity of nutrients in well-illuminated waters restricts the increase in growth rates that could be expected from light stimulation of growth alone. However, in the gyre and upwelling settings illustrated in Figure 7, the small variation in phosphate concentration with depth is not modeled to contribute to significant changes in growth rate.

Unfortunately, in the upwelling and Eastern gyre settings, surface ε_p measurements are not available. However, the model that fits the Pacific central gyre suggests that the observed ε_p values at depth may be several permil lower than those at the surface. The depth of most significant alkenone production and export is uncertain and data is limited (Figure 7B). In the central gyre,

alkenones are most abundant in the deep chlorophyll maximum and coccoliths are abundant throughout the water column (Beaufort et al., 2008; Tolosa et al., 2008). In the Peru upwelling zone, comparable abundances of alkenones occur much shallower, at 40 m, but due to the high chlorophyll abundance, coincide already with low light. Only in the Eastern gyre setting is maximal coccolithophorid abundance found at the very surface-most sample (Beaufort et al., 2008), suggesting shallow production in high light conditions. Nonetheless, these observations represent a single point in time observation, making it difficult to generalize about the absolute light at the depth of maximum alkenone production. It is worth noting that most sampling of water column alkenones in the photic zone (Bidigare et al., 1997) was done from 5 m depth and may sample cells grown at much higher light conditions than average production depths in some settings.

4.2 Simulation of ε_p variations over glacial cycles

Given the controls on ε_p derived empirically from culture study, we revisit the drivers of variation in ε_p over Late Quaternary glacial cycles. Despite the uncertainty over the origin and significance of the DIC effect, on a practical level, the regression using the restricted DIC range encompasses the DIC range encountered throughout the global surface ocean during Late Quaternary glacial cycles, and may be the most appropriate comparison for the CO_2 dependence of ε_p over Quaternary glacial cycles. Using the maximum dependence of ε_p on $\ln([CO_2]_{aq})$ of 2.66, the changes in $[CO_2]_{aq}$ from 5-8 uM would be expected to result in about 1 ‰ rise in ε_p between glacial CO_2 minima and interglacial CO_2 maximum if all other factors (light, growth rate, size) remained constant (Figure 8). The identified changes in cell size produce a comparable range of variability of around 1 ‰ in the two sites in which size is determined (Equatorial Pacific and Western Tropical Atlantic).

All sites feature deviations between measured ε_p and the statistical model based on CO_2 and CO_2 and size (Figure 8). However, unlike the case for the diffusive model, for none of the sites is the model-data deviation correlated with CO_2 aq (Supplemental Figure S6). The variability not explained

by CO_2 and size, according to the predictive model, could arise from variation in light or variation in growth rate. In the Western Tropical Atlantic site, the difference between the modeled ε_p (accounting for size) and the measured ε_p shows only small variations (Figure 8B), suggesting that variations in light and or growth rate were modest, or that increases in light were coupled to decreases in nutrients leading to minimal net effect on ε_p in this location. The small deviations between modeled and measured $\boldsymbol{\varepsilon_p}$ show no correlation with the relative abundance of nannolith *F. profunda* (Supplementary Figure S5), which in core top sediments correlates inversely with higher satellite-detected chlorophyll (Beaufort et al., 1997), and is directly proportional with upper water column stratification (Molfino and McIntyre, 1990). The inverse relationship between stratification and nutrient delivery typical for most open ocean sites may not dominate at this location due to nutrient contributions from the Amazon plume.

In the Equatorial Pacific site, there are larger differences between measured ε_p and the ε_p predicted from CO_2 (Figure 8A) or from CO_2 and size changes, suggestive of more significant variations in growth rate and/or light. Yet, for either model prediction with or without cell size variations, the residual differences are not strongly correlated with % *F. profunda* (Supplementary Figure S5). This suggests that integrated growth rate and light effects may not have a simple relationship with classical indicators of water column stratification and biomass, even in locations where nutrient supply is dominated by periodic destratification.

In the Arabian Sea, the ε_p variation predicted from CO_2 using culture regressions strongly underestimate the amplitude of ε_p variation. Potentially, the natural growth conditions in highly productive high chlorophyll settings with strong light attenuation may differ significantly from the majority of culture experiments. For example, if light enhances the efficiency of CCM, then the coefficient of ε_p dependence on $[CO_2]_{aq}$ may be higher in very low light settings where CCM upregulation is limited. However, the absence of correlation between $[CO_2]_{aq}$ and model-data ε_p deviation suggests that variations in light or growth rate may be the dominant cause of ε_p variation in

this setting, and it is noteworthy that deviations (Figure 8D) broadly follow the low latitude precession cycle known to modulate wind intensity and upwelling in this region (Bassinot et al., 2011).

Finally, at this scale of variation in ε_p (about 1 ‰), it is worth noting that the quality of the reconstruction of $\delta^{13}C_{DIC}$ in the ocean from foraminifera may also contribute to noise in the residuals. Planktic foraminiferal $\delta^{13}C$ may be offset from surface ocean DIC due to size-related vital effects, carbonate ion vital effects, and other processes (Birch et al., 2013), and some differences in $\delta^{13}C$ trends among species have been observed over glacial cycles in the Equatorial Pacific (Spero et al., 2003). All of the cited ε_p values over glacial-interglacial cycles are referenced to $\delta^{13}C$ of *N. dutertrei* which has a habitat in the middle to deep thermocline.

4.3 Implications for ε_p and CO_2 reconstructions

4.3.1 Theoretical caveats of the statistical model

We develop a statistical multilinear regression model to quantitatively parse out the factors (primarily light, growth rate, size, and $[CO_2]_{aq}$), that contribute to carbon isotope fractionation in alkenone-producing algae. The main advantage of this approach compared to the traditional diffusive model is its ability to incorporate the non-linear response of ε_p to changes in $1/[CO_2]_{aq}$, as is observed across culture experiments. The diffusive model further predicts a much steeper slope between ε_p and $1/[CO_2]_{aq}$ at low $[CO_2]_{aq}$ than is supported by the culture data.

However, when transferring this culture-derived relationship to the ocean, there are several challenges, in part due to the limitations of the culture data. First, there is a dearth of culture data at near-modern DIC with aqueous CO_2 higher than ~30 µM. Because our statistical model is calibrated in the window of conditions realistic for the ocean, the statistical regression model may be advantageous compared to the diffusive model for the last several million years when $[CO_2]_{aq}$ was likely less than 30 µM in our tropical downcore locations, but extrapolation to higher $[CO_2]_{aq}$ is likely to be highly uncertain. In general, application of the statistical model to interpret sedimentary ε_p

records is limited by the degree to which culture conditions emulate those of alkenone production in the ocean. Culture experiments are either grown under 24-hour illumination with nutrient limitation, or in a light:dark cycle with excess nutrients, neither of which is representative of tropical oligotrophic environments where light is not continuous and trace nutrients are often limiting. Confidence in our statistical model, and improvements to this empirical approach, could be enhanced in the future if they were derived from conditions more representative of the natural oceanic environments where alkenones are actually produced. A further key uncertainty is the response of carbon concentrating mechanisms to light or trace element limitation in the natural environment, and culture studies evaluating the activity of CCMs under these various limiting conditions would be worthwhile.

4.3.2 Application of the statistical model to Neogene ε_p records

To evaluate the impact of our new culture-constrained statistical model on paleo-pCO_2 estimates, we apply our new method to two tropical sediment sequences and compare the new approach to two published alkenone ε_p records. The test cases are a Plio-Pleistocene record from ODP 925 in the Western Tropical Atlantic (Zhang et al., 2013) and a Neogene record from ODP 999 in the Caribbean Sea (Bolton et al., 2016; Seki et al., 2010). Here we estimate pCO_2 using proxy-derived SST estimates and the measured ε_p values at each site. We incorporate only the minor growth rate variations driven by temperature variations at each site through time. In the absence of constraints on past or present light, we assume an intermediate light (70 $\mu E \cdot m^{-2} \cdot s^{-1}$) and maintain this constant light for all ages and both sites. We then choose the growth rate at each site based on values needed to accurately model the range of glacial-interglacial pCO_2 from ε_p change, for the portion of the record when pCO_2 is known from the ice core record (full model parameters in Supplemental Table S3).

At both sites, the multilinear statistical model produces much more dynamic CO_2 estimates than the conventional diffusive model (Figure 9). Because the diffusive model does not account for the upregulation of carbon concentrating mechanisms with carbon demand relative to carbon

supply, it effectively attenuates the ε_p response. The statistical model evidently improves our ability to quantitatively account for variable CCM activity and more faithfully interpret the ε_p record. At site 925, the conventional diffusion model estimates rather invariant pCO_2 from 0-5 Ma, with a mean estimate around 350ppm for the entire interval and only a very minor trend of 7.6±3.5 ppm CO2 decline/Myr (Figure 9A). Our statistical model calculates higher pCO_2 in the middle Pliocene, and notably reproduces below-modern *p*CO2 in the middle Pleistocene (Figure 9A). The results are in broad agreement with a recent boron isotope *p*CO2 record from planktic foraminifera (Sosdian et al., 2018). The statistical model applied to ODP 999 estimates a similar decline in *p*CO2 over the last 5 Ma (Figure 9B). The average rate of pCO_2 decline in the last 5 Ma from 925 and 999 calculated with the statistical model (32±15; 51±20) is statistically indistinguishable from that calculated from boron isotopes (32±4.7). On longer timescales, the decline in pCO_2 in ODP 999 is even more dynamic, with substantial decline from the Miocene to present. It agrees well with the boron isotope record for much of the 0-16 Ma study interval, but yields higher pCO_2 estimates of around 1000 ppm in the middle Miocene compared to ~500 ppm from foraminifera boron isotopes (Figure 9B). This mid-Miocene value estimated from the statistical model equates to an aqueous CO_2 concentration greater than 30 μM, which is above the concentration for which the statistical model was calibrated, implying a larger but unquantified uncertainty, and thus the absolute values should be interpreted with caution.

4.3.3 Considerations for paleo application

The statistical model, as in previous studies, confirms that multiple environmental factors (e.g. light intensity and cellular growth rate) have as large an influence on ε_p as CO_2 itself. If factors such as light and growth rate vary to as large a degree as they vary in the cultures, extracting the CO_2 component of ε_p variation will indeed be challenging. However, in the ocean, variations in light and nutrients have compensatory effects on growth rate and thus alkenone carbon isotope fractionation: high light niches in the oligotrophic and uppermost photic zone typically have the lowest nutrient concentrations of the surface ocean, while high nutrient niches are often deeper in the upper ocean

and have much lower photon flux densities due to the exponential decay of light energy through the mixed layer. In locations where temporal changes in nutrient supply and growth rate are expected to be large—such as in higher latitude regions affected by the migration of upwelling fronts, or areas where upwelling intensity may vary substantially—robust proxies constraining changes in algal growth rate will be required. Over glacial-interglacial cycles, ε_p has been estimated only from tropical locations; in these locations, the limited set of proxy indicators, such as %*F. profunda* or Cd/Ca, show no significant potential for estimating the net effects of nutrient and light on alkenone carbon isotope fractionation. Many productivity proxies reconstruct whole-ecosystem productivity or export of particulate organic matter, and there is no a priori reason for cellular growth rate at the population level of alkenone producers to be coupled to ecosystem-level trends. Therefore, at present, the multilinear regression model introduced in this study is most likely to be successful where temporal changes in nutrient supply and light intensity are expected to be minimal. In paleobarometry applications that target stable, near-equilibrium regimes, our chosen core sites are likely to have existed under similar broad oceanographic conditions through time. The absolute pCO_2 estimations from the statistical model are highly sensitive to the choice of growth rate (and light); where these can be tuned to match known glacial-interglacial CO_2 variations, then the assumption of constant growth rate allows estimation of pCO_2 in earlier times. In the absence of sedimentary ε_p determinations coeval with independent ice core CO_2 estimates, accurate absolute pCO_2 determinations from pre-Quaternary ε_p would be difficult.

5. Carbon isotopic fractionation in coccoliths as a complementary proxy for CO_2 determinations with ε_p

Our analysis suggests that the relationship between ε_p and CO_2 is conditioned by the upregulation of carbon concentrating mechanisms, and is affected by cell radius, growth rate, light, and potentially DIC. Reconstruction of pCO_2 from measurements of ε_p rests on the potential to

estimate these multiple factors in the past. In this section, we evaluate the potential for the stable isotopic fractionation of C in coccolith $CaCO_3$ to improve the robustness of CO_2 estimates. We describe this fractionation by $\Delta_{cocco\text{-}DIC}$, the difference between coccolith $\delta^{13}C$ and the $\delta^{13}C$ of DIC; in this formulation, a positive $\Delta_{cocco\text{-}DIC}$ indicates coccolith $\delta^{13}C$ is higher than that of DIC.

Carbon isotopic fractionation in coccoliths could improve pCO_2 proxies from coccolithophorids if (a) $\Delta_{cocco\text{-}DIC}$ is a robust predictor of significance of carbon concentrating mechanism (Bolton and Stoll, 2013); (b) Improvement in CO_2 estimates might also be possible if $\Delta_{cocco\text{-}DIC}$ were sufficiently constant, that $\delta^{13}C_{cocco}$ could serve as an indicator for the $\delta^{13}C_{DIC}$ suitable for calculation of ε_p , without need for assuming planktic foraminifera had comparable depth habitats alkenone producers and stable vital effects or without needing to assume constant planktic-benthic $\delta^{13}C$ gradient; (c) improvement in CO_2 estimates might be possible if $\Delta_{cocco\text{-}DIC}$ were a good direct predictor of CO_2 or other variables such as growth rate, light, or DIC that are significant in estimation of CO_2 from ε_p.

5.1 Expected dependence of $\Delta_{cocco\text{-}DIC}$ on $[CO_2]_{aq}$ and HCO_3^- uptake

The precise processes driving isotopic fractionation in coccolithophorids remain debated, because cellular models for C uptake and allocation in coccoliths are under-constrained by experimental data, as described in section 3.2, and because multiple alternative processes can provide viable explanations for observed changes in $\Delta_{cocco\text{-}DIC}$ in cultures. Detailed discussion of potential models of coccolith isotopic composition are provided by several publications (Bolton and Stoll, 2013; Holtz et al., 2017; McClelland et al., 2017). Two key processes that affect isotopic fractionation are fundamental and are manifest in all of the models. First, for a cell of a given size and growth rate, all available models simulate a decrease in the $\Delta_{cocco\text{-}DIC}$ with increasing $[CO_2]_{aq}$. We retain the term *CO_2 effect* for this process, after (Holtz et al., 2017). This response occurs because higher $[CO_2]_{aq}$ results in a greater influx of CO_2 to the cell, effectively diluting the intracellular dissolved C reservoir with isotopically negative C ($\delta^{13}C$ CO_2 ~ -10‰ for DIC of 0‰), which becomes isotopically enriched as photosynthesis preferentially extracts the light isotope and fixes it in organic

matter. In addition to the concentration of aqueous CO_2, this process effectively responds to the C supply relative to demand. For example, for a given $[CO_2]_{aq}$, a higher growth rate will cause a faster isotopic enrichment of the intracellular pool.

Second, if there is an increase in the proportion of HCO_3^- relative to CO_2 crossing the cell membrane, all models simulate an increase in the $\Delta_{cocco\text{-}DIC,}$ because a greater proportion of HCO_3^- will increase the $\delta^{13}C$ of the intracellular reservoir since HCO_3^- has a higher $\delta^{13}C$ than extracellular CO_2. This process was termed the *source effect (Holtz et al., 2017)*. While the consequence of any direct HCO_3^- transport across the cell membrane is clear, there is debate regarding the significance of, and control over, this flux, and the assumption made has important implications for interpretation of $\Delta_{cocco\text{-}DIC,}$. HCO_3^- uptake across the membrane is an energy-consuming process. Some models of phytoplankton suggest that there is a negligible to minor constitutive HCO_3^- flux into the cell that remains constant and is independent of $[CO_2]_{aq}$. These models suggest that carbon concentrating mechanisms regulate the intracellular HCO_3^- transports to the chloroplast, but not the cellular HCO_3^- uptake (e.g. Hopkinson et al 2011, 2014). Such a scenario would be consistent with experimental data from disequilibrium method (Kottmeier et al., 2014) for $[CO_2]_{aq}$ > 5.4 uM. If this were the dominant scenario, then the *CO_2 effect* noted above would be fully expressed. Alternatively, some models suggest that under limiting CO_2, there is an additional transport of HCO_3^- into the cell to support the carbon concentrating mechanism (Holtz et al., 2017; McClelland et al., 2017). Such a scenario would be consistent with experimental data based on MIMS (Kottmeier et al., 2016). Studies suggesting upregulation of HCO_3^- transporters at low $[CO_2]_{aq}$ (Bach et al., 2013) are cited as support for increased HCO_3^- uptake into the cell, however the cellular location of these transporters is not constrained, and may reflect either increased HCO_3^- across the cell membrane or across internal compartment membranes. If upregulation of HCO_3^- transporters in the cell membrane at low $[CO_2]_{aq}$ is the dominant control over cellular HCO_3^- uptake, then a shift from a more significant HCO_3^- source at low $[CO_2]_{aq}$ to a dominant CO_2 source at higher $[CO_2]_{aq}$ would amplify the CO_2 effect.

Finally, some parameterizations of HCO_3^- uptake across the cell suggest it is proportional to the HCO_3^- gradient, and is therefore greater when extracellular HCO_3^- concentrations are higher (Holtz et al., 2015, 2017). If this latter process were important, it could attenuate the CO_2 effect in experiments in which CO_2 is manipulated by varying the DIC concentration, for which high $[CO_2]_{aq}$ also entails high HCO_3^- concentrations, as modeled by Holtz et al (2017). Furthermore, if this latter process were important, then culture experiments conducted at very high DIC and HCO_3^- concentrations may not predict well the $\Delta_{cocco\text{-}DIC}$ in the late Quaternary or earlier periods when DIC concentrations were similar to modern.

5.2 Observations of $\Delta_{cocco\text{-}DIC}$ in constant and variable DIC experiments

Culture experiments with *E. huxleyi* to date provide the most varied experimental matrix in which to examine $\Delta_{cocco\text{-}DIC}$, because they include both experiments with constant modern DIC and those with significant variations in DIC. We focus here on three sets of experiments reporting both ε_p and $\Delta_{cocco\text{-}DIC}$. These include new $\Delta_{cocco\text{-}DIC}$ results (methods described in Supplemental Methods; new data in Supplemental Table S4) for two experiments with *E. huxleyi* at constant pCO_2 and DIC for which analyses of $\boldsymbol{\varepsilon_p}$ have been published and discussed previously (Tchernov et al., 2014), and one published study in which the media DIC concentration varied from 1 to 8 mM (McClelland et al., 2017). The first two experiments manipulated growth rate with temperature (Figure 10A) and light (Figure 10B), and feature only small (13-18 μM) to minimal (13-14 μM) changes in $[CO_2]_{aq}$, but nonetheless significant variations in C demand relative to supply due to growth rate. The third study featured a large range in $[CO_2]_{aq}$ (5 to 42 μM) and minimally varying high growth rates, and about double the range in C demand/supply (Figure 10C).

Evidence of a *CO_2 effect*, with increasing $\Delta_{cocco\text{-}DIC}$ with increasing demand/supply, is most clear in the experiments with large range in DIC and $[CO_2]_{aq}$ (Figure 10C) and limited variation in growth rate. Experiments with $[CO_2]_{aq}$ less than 13 μM feature a much higher $\Delta_{cocco\text{-}DIC}$ than experiments with $[CO_2]_{aq}$ greater than 15 μM (Figure 10C). Because DIC varies significantly in these experiments, the CO_2 effect may be attenuated due to the source effect if there is cellular HCO_3^- uptake in

proportion to its abundance in the growth medium. In contrast, the other two culture experiments (Figure 10A, B) show no clear evidence of a CO_2 effect, although they span a range in C supply/demand comparable to the range in which the effect is evident in the DIC cultures (Figure 10C). Both cultures at constant DIC (Figure 10A,B) show no significant trend in $\Delta_{cocco\text{-}DIC}$ with C demand/supply, even though the temperature experiments (Figure 10A) feature a 9 ‰ decrease in ε_p with increasing C demand/supply. Due to the low range in $\Delta_{cocco\text{-}DIC}$ in this experimental series (Figure 10A), while ε_p alone is a strong predictor of $[CO_2]_{aq}$ (r^2= 0.68); the paired measurement of $\delta^{13}C_{cocco}$ and $\delta^{13}C_{POC}$ without need for expressing fractionation relative to $\delta^{13}C_{DIC}$ or $\delta^{13}C_{CO2}$, was a slightly better predictor of $[CO_2]_{aq}$ (r^2=0.73). Models suggest multiple processes that may attenuate the expression of the *CO_2 effect* in culture experiments with variable growth rate and constant CO_2, such as a constant low constitutive HCO_3^-influx to the cell, which eliminates potential for the source effect, and HCO_3^- transport to the chloroplast with a constant proportion to fixation. Among these three experiments, the *CO_2 effect* is manifest most clearly in the experiments with highest average P_{var} (range is 3.3x 10^{-5} to 3.7 x10^{-4} in Figure 10C, compared to 3.4 x10^{-6} to 4.8x10^{-5} in Figures 10A and 10B). The higher P_{var} may be indicative of a more extensive operation of CCM; however, in the absence of quantitative mechanistic models, the existence of the *CO_2 effect* is not necessarily diagnostic of the operation of CCM.

The experiments with light modulation of growth rate (Figure 10B) suggest the potential for an independent influence of light on $\Delta_{cocco\text{-}DIC}$. The highest $\Delta_{cocco\text{-}DIC}$ are attained in high light conditions (Figure 10B). Among two experiments with similar low supply/high demand, increasing light from 80 to 120 $\mu Em^{-2}s^{-1}$ results in a 1 to 1.5 permil increase in $\Delta_{cocco\text{-}DIC}$. In contrast, in experiments at nearly constant light (68-87 $\mu Em^{-2}s^{-1}$) where growth rate varies with temperature, there is no significant trend in $\Delta_{cocco\text{-}DIC}$ with growth rate, either positive or negative (Figure 10A). Although the number of data is limited, this comparison suggests that increased light, and not growth rate itself, may cause increase in $\Delta_{cocco\text{-}DIC}$. Therefore the effect we observe may be different from the *light effect* as

described by (Holtz et al., 2017), which was a manifestation of higher light leading to higher growth rates and higher C demand relative to supply, which we have described as part of the *CO_2 effect*.

The high light experiments in Figure 10B also feature high calcite/cell and high calcification rates. A correspondence between high light and high cellular calcification was noted previously for these culture experiments (Stoll et al., 2002) and others experiments with *E. huxleyi (Rost et al., 2002)*. The observation that ε_p is higher in higher light cultures has been extensively commented, as discussed in section 4.1.2. In this particular culture study shown in Figure 10B, it was suggest that high light stimulates massive carbon cycling, a light-dependent influx and efflux of inorganic carbon independent from carbon fixation (Tchernov et al., 2014). One function suggested for coccoliths is protection from photoinhibition at high light conditions, and also energy dissipation in high light conditions (Monteiro et al., 2016). Such a linkage may contribute to the correlation with cellular calcification and light, and the potential influence of light on $\Delta_{cocco\text{-}DIC}$ independent of growth rate, warrants further investigation.

5.3 Variation in $\Delta_{cocco\text{-}DIC}$ over the late Quaternary CO_2 Cycles

We evaluate next if there is evidence for the *CO_2 effect* or CCM operation on $\Delta_{cocco\text{-}DIC}$ over glacial CO_2 cycles, given atmospheric pCO_2 variations from 180 to 287 ppm over the last 250 ka (Petit et al., 1999), and estimating $[CO_2]_{aq}$ for surface ocean waters in equilibrium with the atmosphere at the sea surface temperature independently estimated for each site and age. Our evaluation includes two tropical sites, which have $[CO_2]_{aq}$ variations in the range from 5 to 8 μM, and one mid-latitude site with $[CO_2]_{aq}$ variations in the range from 6 to 10.5 μM.

In evaluating $\Delta_{cocco\text{-}DIC}$ in coccoliths isolated from sediments, two challenges must be acknowledged. First, because different species have different absolute values of $\Delta_{cocco\text{-}DIC}$, identification of trends within a given species requires careful separation of coccoliths by size, and where possible, by species (Stoll, 2005; Stoll and Ziveri, 2002). In practice, such separation can be challenging, and the species composition of a given size fraction may vary over time as environmental factors influence the community composition. To overcome this challenge as

effectively as possible, we code the subsequent figures with information about the coccolith assemblage in the analyzed sample. Our assumption is that trends between $\Delta_{cocco\text{-}DIC}$ and environmental factors that are evident in samples with very similar assemblages, are likely due to environmental factors rather than mixing of coccoliths with different composition. The second challenge is that, analogous to the estimation of ε_p, the inference of $\delta^{13}C_{DIC}$ must be made from planktic foraminifera, and often the species and size fraction available or measured differs between locations. There is still some debate regarding absolute corrections for planktic foraminiferal $\delta^{13}C$ vital effects in different species and size fractions. Consequently, we report here simply $\Delta_{cocco\text{-}foram.}$ and identify the foraminifera employed as the reference. We focus on comparing trends and the ranges of variability between sediments and culture experiments, rather than comparing the absolute values of $\Delta_{cocco\text{-}foram.}$

In the Western Tropical Atlantic site, for sediments covering the last 105 ka, two fractions were produced in the 3-5 μm range. Both fractions are numerically dominated (~50%) by the species *Gephyrocapsa*; however, the larger fraction also has frequent *H. carteri*, and the smaller fraction also has significant *U. sibogae* (symbols coded for accessory species abundance in Figure 11A). Both fractions exhibit a ~ 1 ‰ range over the last glacial cycle. When comparing samples of comparable species composition (comparable color symbol), lower $\Delta_{cocco\text{-}foram}$ characterizes the higher CO_2 interglacial periods, consistent with the *CO_2 effect*. A similar trend of minimum $\Delta_{cocco\text{-}foram.}$ is seen in the *Gephyrocapsa*-dominated (75-90% *Gephyrocapsa* numerically) from Somali Basin NIOP 905 (Figure 11B) where sediments of age of the last 33 ka were separated. Similar to the Western Tropical Atlantic, the change in $\Delta_{cocco\text{-}foram}$ is most pronounced between intermediate and high CO_2, rather than lowest and highest CO_2. Similar trends have been described in bulk carbonate fractions from Caribbean sediments over the last glacial cycle, although quantitative counts of the species composition are not available (Hermoso, 2016). Bulk coccolith fractions spanning the interval 200 to 110 ka, with quantitative species counts estimating the $CaCO_3$ contribution by each species, have been measured in sediments from the Agulhas Basin (Mejía et al., 2014) (Figure 11C). Within a

similar assemblage composition, generally higher CO_2 interglacial periods are also characterized by lower $\Delta_{cocco\text{-}foram,}$ as observed in the W. Tropical Atlantic and Somali Basin. During the CO_2 maximum at MIS 5e, this trend is less clear. Potentially in this higher latitude site of higher $[CO_2]_{aq}$, or in these bulk sediments with carbonate dominantly from larger, more heavily calcified coccoliths, other factors become dominant. Alternatively, glacial temperature changes in higher latitude regions may exert a greater effect on growth rates, with maximum temperatures during the peak MIS5e stimulating higher growth rates which decrease the C supply/demand ratio. The highest growth rates of the entire record have been inferred for the MIS 5e period (Mejía et al., 2014)

In the warm tropical oceans, $\Delta_{cocco\text{-}foram}$ appears to manifest the CO_2 effect over glacial-interglacial CO_2 cycles, where $[CO_2]_{aq}$ variations are in the range of 5 to 8 μM. The expression of this effect implies that the proportional changes in CO_2 over time are greater than, or anticorrelated with, temporal changes in growth rate in these locations, so that CO_2 increase also entails a net increase in C supply/demand. The expression of this nearly ~ 1 ‰ shift over just a few μM change in $[CO_2]_{aq}$ implies a very high sensitivity. However, culture data for *E. huxleyi* manifest a very high sensitivity over a narrow, albeit higher (12 to 15 μM) CO_2 range (Figure 11D green symbols). The higher range of this threshold in the culture study may reflect the very high light and absolute growth rates, or the interaction of varying DIC and CO_2 on the source effect. As better experimental data provide tighter constraints on cellular carbon isotope fractionation models, it may be possible to further interpret the variation in $\Delta_{cocco\text{-}DIC}$ over glacial $[CO_2]_{aq}$ cycles. For example, with cellular models, it may be possible to assess whether $\Delta_{cocco\text{-}DIC}$ variation indicates increased HCO_3^- uptake by the cell at low glacial $[CO_2]_{aq}$, or whether it provides evidence for substantial variations in growth rate.

5.4 Interspecific vital effects and change in $\Delta_{cocco\text{-}DIC}$ of large, heavily calcified coccoliths in cultures and on long timescales

In contrast to the data from glacial/interglacial cycles, on longer multi-million year timescales the $\Delta_{cocco\text{-}DIC}$ of large, heavily calcified coccoliths has been suggested to positively covary with $[CO_2]_{aq}$ (Bolton et al 2016). The range in vital effects between small and large coccoliths has also been

suggested to positively covary with $[CO_2]_{aq}$ (Bolton and Stoll, 2013; Hermoso et al., 2016; Rickaby et al., 2010; Stoll, 2005; Tremblin et al., 2016; Ziveri et al., 2003). While earlier culture studies had suggested that under CO_2 limitation, small coccoliths had a more limited range of $\Delta_{cocco\text{-}DIC}$ (Hermoso et al., 2016), a compilation of all available published data for small (e.g. cells producing coccoliths estimated to be in the 3-5 μm range) and intermediate (e.g. cells producing coccoliths estimated to be in the 5-8 μm range), shows no systematic difference in the range of variation they experience across the full spectrum of $[CO_2]_{aq}$ (Figure 12A). In particular, high variability is seen in the small (3-5 μm) coccoliths at $[CO_2]_{aq}$ <20 μM. In contrast, culture studies suggest systematic increases in $\Delta_{cocco\text{-}DIC}$ of *C. pelagicus* and *C. leptoporus* with increasing DIC or $[CO_2]_{aq}$ (Figure 12B; r^2 = 0.82 with DIC, r^2 = 0.89 as multiple regression DIC and radius). This latter relationship , is appealing as a potential direct indicator of $[CO_2]_{aq}$, if indeed driven by $[CO_2]_{aq}$ and not DIC, and if the uncertainties in estimation of $\delta^{13}C_{DIC}$ from foraminifera are sufficiently small. A direct dependence of $\Delta_{cocco\text{-}DIC}$ on $[CO_2]_{aq}$ in large coccoliths has been attributed to reallocation of HCO_3^- between calcification and photosynthesis (Bolton and Stoll, 2013), or to Rayleigh distillation within the coccolith vesicle (McClelland et al., 2017). Alternatively, if the relationship is driven by higher HCO_3^- transport into the cell at higher media DIC, it may reflect DIC concentrations rather than $[CO_2]_{aq}$.

Over the latest Miocene $\Delta_{large\ cocco\text{-}foram}$ declines (Bolton et al., 2016), in concert with decline in atmospheric CO_2 estimated from diatom ε_p (Figure 12D; Mejia et al., 2017). In this particular record, $\Delta_{small\ cocco\text{-}foram}$ has a smaller variation, so $\Delta_{large\ cocco\text{-}small\ cocco}$ yields a similar trend. The magnitude of decline in $\Delta_{large\ cocco\text{-}foram}$ (2 ‰) is about 2/3 of the range observed across culture experiments. In the range of low $[CO_2]_{aq}$, this would be equivalent to CO_2 decline from about 25 to 10 μM. If driven by DIC, this would be equivalent to a ~twofold reduction in DIC.

Over the Eocene-Oligocene Transition, $\Delta_{large\ cocco\text{-}small\ cocco}$ suggest a slight long term decline of approximately 1 ‰ (Figure 12C) (Tremblin et al., 2016). In contrast, $\Delta_{large\ cocco\text{-}DIC}$ declines by nearly 2 ‰ through the latest Eocene, with a local minimum across the EOT (Figure 12D). DIC $\delta^{13}C$ was calculated from benthic foraminfera and assumption of a stable benthic-planktic $\delta^{13}C$ gradient

(Pagani et al., 2011; Zhang et al., 2013). If $\Delta_{\text{large cocco-DIC}}$ is substantiated as a direct CO_2 indicator, and the DIC estimation technique is robust, then this variation suggests CO_2 decline closely following temperature change across the late Eocene to early Oligocene. Alternatively, this could reflect DIC decline and the climatic correlation may reflect coupling between DIC and atmospheric pCO_2.

Overall, while $\Delta_{\text{large cocco-DIC}}$ may hold significant potential for identifying changes in CO_2, the absence of experiments at elevated CO_2 but close to modern DIC makes it difficult to distinguish effects of CO_2 limitation from potential influence of seawater DIC on the HCO_3^- uptake by cells. A range of culture experiments with large, heavily calcified coccoliths, with an experimental matrix more closely matched to the likely ranges of variations in the carbon cycle in the Cenozoic is required to clarify the potential utility of this indicator, and the potential for effects of light and growth rate to modulate the relationship between $\Delta_{\text{large cocco-DIC}}$ and CO_2 or DIC.

6. Implications and conclusions

Published alkenone ε_p records spanning known glacial CO_2 cycles, show considerably less variability than predicted by the diffusive model for cellular C acquisition, given reasonable estimations of variations in growth rate and cell size and the standard assumption of constant cell membrane permeability to CO_2. However, the discrepancy between the diffusive model and observations is not limited to natural samples over glacial cycles but also occurs in experimental culture of coccolithophorids as well as diatoms. The discrepancy can be quantified as the effective cell CO_2 permeability required to match the diffusive model, revealing that a higher CO_2 permeability is required at low availability of CO_2 relative to cellular carbon demand. Comparison with detailed models of diatom isotopic fractionation, membrane permeability, and carbon acquisition suggests that rather than extreme variations in cell membrane permeability, phytoplankton cells under CO_2 limitation might accomplish a comparable high throughput of C to an intracellular compartment where the photosynthetic enzyme is housed, through the operation of carbon concentrating mechanisms. Such carbon concentrating mechanisms are ubiquitous in all classes of phytoplankton

and likely represent the actual physical process responsible for deviation of coccolithophorid isotope fractionation from diffusive models.

Rather than a hyperbolic relationship between ε_p and CO_2 suggested by the diffusive model, experimental data from laboratory culture suggest a power relationship between ε_p and CO_2. Multiple regression models demonstrate that many of the variables described in the diffusive model (radius, growth rate) are important predictors of ε_p; but light and experiment DIC also affect ε_p. Regression models for laboratory culture data imply a much smaller dependence of ε_p on $[CO_2]_{aq}$ in the low $[CO_2]_{aq}$ range, than inferred from the hyperbolic form of the diffusive model. This suggests that detection of small variations in $[CO_2]_{aq}$ in the low $[CO_2]_{aq}$ range, may remain challenging, especially if the other factors (light, growth rate, cell size) experience appreciable variations at a given oceanographic setting. Searching for oceanographic settings where such variables can be either stable or well-constrained may enhance the detection of CO_2 component in ε_p.

The statistical regression model derived for cultures is applied to estimate pCO_2 from the Late Miocene to present from ε_p at two tropical locations (ODP 925 and ODP 999) that have previously been suggested to have experienced minimal long-term changes in general oceanographic conditions and algal growth rate. The statistical regression model estimates a much more dynamic range in pCO_2 than the classic diffusive model, identifying a significant decline in pCO_2 in the last 5 Ma, which is comparable to that estimated from boron isotopes of foraminifera. Although significant challenges remain in the estimation of absolute growth rates and light levels characterizing past production by alkenone producers, the statistical model offers an approach for estimating pCO_2 for recent periods of relatively low atmospheric pCO_2 (e.g. within the calibration range) at sites likely to have experienced limited variation in growth rate and algal productivity dynamics, and when the effective growth rate can be locally tuned to ice core CO2 using ε_p determinations in sediments spanning the last 800 ka.

Carbon isotopic fractionation in coccoliths has previously been suggested as a complementary proxy for estimating CO_2 together with ε_p. Multiple sites from tropical and subtropical locations

suggest a trend toward lower $\Delta_{cocco\text{-}foram}$ during high CO_2 interglacials than during low or intermediate CO_2. Such a trend could be consistent with a strong influence of the passive CO_2 diffusive influx into cells, altering the isotopic composition of the internal cellular C pool. This interpretation would imply a high sensitivity of coccolith $\delta^{13}C$ in this low CO_2 range. Further experimental calibration of this isotopic dependence, combined with strong experimental constraints on cellular carbon models, may enable these signals to be quantitatively interpreted in the future. In particular, model studies would be useful to elucidate whether this fractionation trend requires upregulation of cellular HCO_3^- uptake during glacial CO_2 minima.

The small amplitude of ε_p variations over glacial CO_2 cycles has led some to question the reliability of ε_p for reconstruction of long-term CO_2. However, the $[CO_2]_{aq}$ in the tropical oceans during glacial CO_2 minima represents the most extreme CO_2 minima likely experienced by phytoplankton in the Cenozoic, and hence an end-member scenario favoring more extreme upregulation of the carbon concentrating mechanism. Our analysis suggests that a potential dependence of cellular C uptake on DIC concentration could potentially lead to underestimation of the sensitivity of ε_p to CO_2 when culture experiments at high CO_2 and DIC are used to predict the ε_p to CO_2 relationship in past oceans for which some models suggest much more limited variation in DIC (Hain et al., 2015; Zeebe, 2012). Regressions based on cultures identify an overall higher sensitivity of ε_p to CO_2 than predicted by the diffusive model, particularly in the range of >20 μM $[CO_2]_{aq}$. However, culture data suggest that the effects of light and growth rate on ε_p may be large. To attain robust quantitative pCO_2 estimates from phytoplankton $\varepsilon_{p,}$ either better proxy records for light and growth rate effects are needed, or further work in the ocean water column is required to elucidate how regulation of phytoplankton growth may minimize the natural parameter space in which the most significant coccolithophorid production occurs, due to interactions among light and nutrient limitation and temperature effects on growth rate.

Acknowledgements

We thank Lydia Bailey and Madalina Jaggi for assistance in laboratory. This research was supported by the ETH Zürich.

Table 1. Sources of data from laboratory cultures of coccolithophorids (Bidigare et al., 1997; Hermoso et al., 2016; McClelland et al., 2017; Rickaby et al., 2010; Riebesell et al., 2000b; Rost et al., 2002; Tchernov et al., 2014). Studies which report both isotopic data on organic matter and coccoliths are indicated in purple; studies with only isotopes on POC are in red, and studies with only isotopes in coccoliths are in blue. Although estimations of coccolith $\delta^{13}C$ were also made by Rost et al. (2002) based on the difference between $\delta^{13}C$ POC and $\delta^{13}C$ total particulate carbon (TPC); such an approach accumulates uncertainties in the estimates of TPC, POC, and PIC. One study (Rickaby et al 2010) presents data from both methods and shows that directly measured $\delta^{13}C$ coccolith is variously higher or lower than that calculated from $\delta^{13}C$ POC and $\delta^{13}C$ TPC by up to 3 permil, so the estimated $\delta^{13}C$ coccolith from Rost et al (2002) is not included in our analysis. Only a few studies report $\delta^{13}C$ DIC determinations made on each experimental culture treatment; of these, only one (Rickaby et al., 2010) reports $\delta^{13}C$ DIC at both the start and end of the experiment; the variation was up to 1 ‰. Variation in closed batch cultures is due to removal of organic carbon from DIC, and alteration of media carbon chemistry by photosynthesis and calcification, and this evolution could be sensitive to cell density and PIC/POC. Other studies measure $\delta^{13}C$ DIC on an initial media batch and report this value for each experimental treatment, assuming that this $\delta^{13}C$ DIC is constant over the adjustment of culture media and the duration of culturing. Where no radius or POC/cell is available, cell radius was subsequently estimated using the radius reported in other publications for that species and strain from the same laboratory (e.g. for study 1, radius taken from (Popp et al., 1998b); for study 7, radius taken from study 8); for study 5, radius was estimated using N quota and C:N ratio assuming a relationship between cellular radius and C quota from Popp et al., 1998b.

		SPECIES					PROXY				FORCING RANGES					CULTURE MEASUREMENTS				
	Data source	*E. huxleyi*	*G. oceanica*	*C. pelagicus*	*C. leptoporus*	*Other*	δ13C POC	δ 13C calcite	$\delta^{13}C$ DIC each experiment	$\delta^{13}C$ DIC initial batch	Light (µE.m2/s)	Photoperiod duration (hours)	Temperature	DIC range (mM)	pH range	Growth rate	Radius from POC/cell	Radius from coccosphere diameter	PIC/cell	PIC/POC
1)	Bidigare 1997	x					x		x		250	24	18			x				
2)	Riebesell 2000	x					x		x		150	16	16	2-9	8.1-9.1	x	x			
3)	Rost 2002	x					x		x		15-150	24,16	15	2.6	7.9-8.6	x	x		x	X
4)	Rickaby 2010		x	x			x	x	x		200	16	18	1-8	7.9-8.2	x	x		x	x
5)	Tchernov 2014	x					x	x	x		9-123	24	7-18	2.1	8.1	x			x	
6)	McClelland 2017	x	x	x			x	x		x	250	12	15	1-12	8.2	x	x		x	x
7)	McClelland 2017 (MH)		x					x		x	250	12	15	0.5-24	8.2					
8)	Hermoso 2016	x		x	x	x		x		x	150	14	15	2-12	8.2	x		x		

.

Table 2: Results from regression models

ε_p ~ (ln)CO_2+(ln)light+ μ_i + radius (a)

Full culture dataset (n= 153); R^2= 0.68

	coeff	lower CI	upper CI	p value
Intercept	10.42	7.77	13.06	1.1E-12
(ln)CO_2	1.45	0.85	2.04	3.4E-06
(ln)light	2.00	1.38	2.61	2.1E-09
μ inst	-6.27	-7.19	-5.36	1.3E-27
radius	-1.41	-1.64	-1.19	2.2E-25

ε_p ~ (ln)CO_2+(ln)light+μ_i+ radius+(ln)DIC (b)

Full culture dataset (n= 153); R^2= 0.70

	coeff	lower CI	upper CI	p value
Intercept	9.07	6.37	11.77	5.8E-10
(ln)CO_2	2.38	1.57	3.20	4.4E-08
(ln)light	2.04	1.44	2.64	3.9E-10
μ (instantanteous)	-6.08	-6.98	-5.19	3.2E-27
radius	-1.42	-1.64	-1.21	1.6E-26
(ln)DIC	-1.69	-2.73	-0.64	1.7E-03

ε_p ~ (ln)CO_2+(ln)light+ μ_i + radius (c)

DIC 1.6-3 mM culture data (n= 100); R^2= 0.71

	coeff	lower CI	upper CI	p value
Intercept	6.26	2.92	9.60	3.3E-04
(ln)CO_2	2.66	1.83	3.50	7.6E-09
(ln)light	2.33	1.69	2.96	8.6E-11
μ (instantanteous)	-6.98	-8.16	-5.81	2.7E-20
radius	-1.28	-1.71	-0.84	7.8E-08

Figure Captions

Figure 1. Comparison of measured ε_p (blue circles) and that predicted by the diffusive model in four locations spanning glacial-interglacial CO_2 variations. ε_p is measured as the difference in carbon isotope ratios between the dissolved aqueous CO_2 and algal organic matter and the, which is inferred from the carbon isotope ratios of coeval planktic foraminifera. A) core W8402-14 GC, Equatorial Pacific, B) core ODP 925, Western Tropical Atlantic, C) core GeoB 1008, Angola basin, and D) core NIOP464, Western Arabian Sea; see Supplementary Figure S1 for map. Also shown is the $[CO_2]_{aq}$ in equilibrium with atmospheric CO_2 from ice core records and proxy sea surface temperature at each location (black line). Diffusive model ε_p use mean alkenone producing radius of 1.81 μm (global Holocene average from Bollman et al. (2002)), unless noted otherwise. Red squares show diffusive model prediction with growth rate take from modern constant PO_4 and proxy temperature, using the growth rate dependence on PO_4 and temperature from Krumhardt et al. (2017), and a permeability of $5.2 \cdot 10^{-5}$ $m \cdot s^{-1}$which provides the lowest discrepancy between average modeled and measured Holocene ε_p values. Green symbols show model result using mean cell diameter estimated from coccolith length. Purple symbols show model result using variable PO_4 concentrations, derived from proxy records in each core: % *F. profunda* in Equatorial Pacific and Western Tropical Atlantic (regression *F. profunda* vs PO_4 from Hernandez-Almeida et al., 2018), planktic foraminiferal Cd/Ca in Arabian Sea; and $\delta^{15}N$ in the Angola Basin (Holmes et al., 1997). All data are given in Supplemental Table S1. The difference between observed and modeled ε_p is significantly correlated (p value $<1x10^{-4}$) to $[CO_2]_{aq}$ in all sites except the Angola basin.

Figure 2. For low latitude sites (< 35° North or South) with temperature >23 °C. The relationship between ε_p and $[CO_2]_{aq}$ in situ. Colors show the measured $[CO_2]_{aq}$ minus the $[CO_2]_{aq}$ at equilibrium with atmosphere at time of sampling. The data include locations from Equatorial Pacific, Equatorial Pacific Iron Fertilization, Bermuda Time Series, and Arabian Sea campaigns described in (Bidigare et al., 1997; Laws et al., 2001).

Figure 3. Measured ε_p, versus the carbon availability: $[CO_2]_{aq}$ (mol $C \cdot m^{-3}$) * surface area(m^2) relative to demand by fixation (mol C s^{-1}). The carbon availability relative to demand could be converted to a dimensionless ratio of C supply to demand if a permeability estimation were included in the numerator to convert C availability to a flux. When permeability is not incorporated in the numerator, as here, the net units are $s \cdot m^{-1}$. Blue circles correspond to culture experiments summarized in Table 1 and red circles to data obtained from sediments spanning glacial-interglacial cycles, as plotted in Figure 1. Orange curves show the diffusive model fit for different permeability values, as labeled on each curve.

Figure 4. Panels A) and B) show the permeability value required by the diffusive model to attain the measured ε_p versus the CO_2 availability ($[CO_2]_{aq}$ * surface area) relative to demand by fixation; units identical to figure 3. A) Value calculated from sedimentary alkenones from sites illustrated in Figure 2, assuming constant growth rates at each site through time. B) Value calculated

for all published alkenones produced in culture, as tabulated in Table 1. Yellow shading shows the range of passive (dark) cell membrane permeability among four species of diatoms measured by Membrane Inlet Mass Spectrometry (Hopkinson et al., 2011). Bars show the average and range of values inferred from each species of coccolithophorid. The yellow star indicates the highest CO_2 experiment (274 μM $[CO_2]_{aq}$) of (Bidigare et al., 1997) study listed in Table 1. In Figure 4b, blue shading shows the range of sediment-derived values shown in Figure 4a.

Figure 5. A-B) schematic diagram of single compartment cell, as used in the diffusive model, comparing high and low permeability situation. C) - D), Schematic of two-compartment cell with a chloroplast/pyrenoid region, illustrating the difference between highly active chloroplast pump with high active HCO_3^- influx to chloroplast (High CCM) and a weaker chloroplast pump with lower active HCO_3^- influx to chloroplast (Low CCM, E) Permeability value required by the diffusive model to attain the measured ε_p, plotted versus the CO_2 availability ($[CO_2]_{aq}$ * surface area) relative to demand by fixation (units identical to Figure 3), for cultured diatom *P. tricornutum* data as compiled in Riebesell et al. (2000) with distinct symbols for nutrient and light-limited experiments. F) Modeled active HCO_3^- transport to the chloroplast required to match the observed ε_p of cultured diatom *P. tricornutum* data as compiled in Riebesell et al. (2000) using a two-compartment cellular model for diatoms, calculated as described in Mejia et al. (2017). Lines indicate the range of passive (dark) cell membrane permeability for four species of diatoms measured by Membrane Inlet Mass Spectroscopy (Hopkinson et al., 2011).

Figure 6. A) Sensitivity of ε_p to light ($\mu E \cdot m^{-2} \cdot s^{-}$) and B) ε_p to $[CO_2]_{aq}$, in the final regression model in the dataset with DIC between 1.6 and 3 mM showing the best fit slope (red) and the 95% CI on the slope (gray shading). Coefficients given in Table 2. In B), the black line indicates the relationship predicted by the diffusive model for permeability of 5.2 x 10^{-5} $m \cdot s^{-1}$ and a growth rate of 0.6 day^{-1}.

Figure 7. Distribution of light, coccoliths and alkenones, and alkenone ε_p in the water column in three locations in the Pacific samples in the BIOPE cruise– in the main gyre, the Peru coastal upwelling, and the Eastern Gyre, using data from Beaufort et al. (2008), and Tolosa et al. (2008). The depth axis for each region is given at the left. A) Average light intensity during photoperiod, inm. B) Abundance of coccoliths (blue stars) and alkenones (orange circles) at each depth sampled, with number listing light at depths of maximum coccolith abundance. C) Measured alkenone ε_p at each depth (black symbols). Thin dashed line shows the predicted ε_p decrease when the direct effect of light on ε_p is estimated using the light for each depth, assuming constant growth rate. Solid line shows the net predicted ε_p decrease when the direct effect of light on ε_p is combined with a weak dependence of growth rate on light, ($\mu = 0.15 * \ln(\text{light})$. Thick dashed line in upper panel shows the net predicted ε_p decrease when the direct effect of light on ε_p is combined with a strong dependence of growth rate on light ($\mu = 0.43 * \ln(\text{light})$). Both growth rate dependencies yield similar low growth rate at 1% irradiance, but the latter dependence leads to nearly threefold higher growth rates in the surface. Nutrient influence on growth rate is not included in calculation.

Figure 8. A) to D) Variation in ε_p expected due to variation in $[CO_2]_{aq}$, according to the statistical regression model (red line) based on culture data with DIC between 1.6 and 3 mM for the four sediment cores shown in Figure 1. Parameters used in statistical model are given in Supplemental Table S1; they include growth rate adjusted at each site to give the ε_p value for Holocene (except Western Tropical Atlantic which has no Holocene ε^p) and maintain a constant growth rate and instantaneous light (70 $\mu E \cdot m^{-2} \cdot s^{-1}$) for all remaining ages. Green symbols are calculated as with the red curves, but accounting for variations in the mean coccolith size. Blue symbols show the measured ε_p for each site. Also shown is the $[CO_2]_{aq}$ in equilibrium with atmospheric CO_2 from ice core records and proxy sea surface temperature at each location (black line). Crosses show the difference between observed and statistical model ε_p, which is not significantly ($p<0.05$) correlated to $[CO_2]_{aq}$ for any of the four sites.

Figure 9. Estimated atmospheric pCO_2 for the last 5 Ma (A) and last 16 Ma (B) based on application of the statistical model to published ε_p and temperature records from tropical sites ODP 925(squares) and ODP 999 (circles) (Bolton et al., 2016; Seki et al., 2010; Zhang et al., 2013). pCO_2 calculated using the statistical model (dark blue circles and dark blue squares) and assuming constant light, with only minor growth rate variations predicted from the paleotemperature and assuming constant cell radius (full model parameters listed in Supplemental Table S3). Vertical bars on symbols show the variation in pCO_2 resulting from applying the upper and lower 95% confidence interval on the coefficient between $[CO_2]_{aq}$ and ε_p as listed in Table 2c. Absolute growth rates were scaled so that calculated pCO_2 during the last 800 ky would fall in the range of pCO_2 variation recorded by ice cores. Smaller turquoise symbols show the statistical model calculated as described above, but additionally with variation in cell radius estimated from linear interpolation of cell radius estimates made from coccolith length at ODP 925 (brown x symbols; (Bolton et al., 2016). Black crosses show the pCO2 calculated from the ε_p using classic diffusive models and assumption of constant size and growth rate in A) for ODP 925 as reported by (Zhang et al., 2013) including gray shading for the reported maximum and minimum pCO_2, and in B) for ODP 999 assuming a constant b value of 105. Green shading indicates the 95% confidence interval on pCO_2 estimated from boron isotopes (Sosdian et al., 2018), and in B) small green x symbols denote the ages of boron isotope pCO_2 estimations. Y axis follows a natural log scale to highlight the expected relationship between pCO_2 and climate sensitivity.

Figure 10. A) Results from *E. huxleyi* cultures at constant light, variable temperature and $[CO_2]_{aq}$, B) variable light (10-123 $\mu E \cdot m^{-2} \cdot s^{-1}$) and constant $[CO_2]_{aq}$, and variable DIC and $[CO_2]_{aq}$, details of culture experiments given in Stoll et al., 2001 and Tchernov et al 2014 and Supplementary Methods. C) *E. huxleyi* cultures at variable DIC and constant light, data from McClelland et al., 2017. Lower part of each panel shows forcing for the experiment (temperature °C, light in $\mu E \cdot m^{-2} \cdot s^{-1}$, and DIC in mM), the culture growth rate day^{-1}, calcification (when measured; as pgC/cell or molar PIC/POC ratio), and $[CO_2]_{aq}$ μM. Upper portions of each panel show $\Delta_{cocco\text{-}DIC}$, in B) colors indicate light ($\mu E \cdot m^{-2} \cdot s^{-1}$) and in C) colors indicate $[CO_2]_{aq}$ (μM). Also shown ε_p and the P_{var} (m/s), permeability required to match measured ε_p with the diffusive model.

Figure 11. Isotopic fractionation in coccoliths, expressed relative to coeval planktonic foraminifera as indicator of DIC, from periods covering glacial/interglacial oscillations in $[CO_2]_{aq}$. A) From site 925, Western Tropical Atlantic, samples numerically dominated by *Gephyrocapsa*. Color coding indicates the efficiency of separation by species: variation in red colors shows a larger fraction and the relative abundance in that size fraction by *H. carteri* which ranges from 14 to 60%. Variation in blue colors shows a smaller size fraction and the relative abundance in that size fraction of *Umbilicosphaera sibogae*. $\delta^{13}C$ DIC is taken from Zhang et al (2013) and is based on foraminifera *G.sacculifer*. B) From Somali Basin NIOP 905,*Gephyrocapsa* dominated size fraction, referenced to stable isotopes in *N. dutertreii (Ivanochko et al., 2005)*. Symbols show relative abundance of small *Calcidiscus leptoporus* in the size fraction. C) Record of coccolith fraction (<20 μm) carbonate from Agulhas Basin (Mejia et al., 2014) The relative carbonate contribution of different species during MIS 5, specifically MIS 5e, are shown in red tones, and relative carbonate contribution of different species for MIS 6 are shown in blue tones. D) Results from *E. huxleyi* cultures at variable $[CO_2]_{aq}$ with DIC manipulation (McClelland et al., 2017). Green symbols correspond to $\Delta_{cocco\text{-}DIC}$ whereas black symbols correspond to P_{var} (m/s), permeability required to match measured ε_p with the diffusive model. $[CO_2]_{aq}$ in μM.

Figure 12. Isotopic fractionation in larger, heavily calcified coccoliths vs smaller coccoliths. A) $\Delta_{cocco\text{-}DIC}$ vs $[CO_2]_{aq}$ for all published culture data from cells expected to produce coccoliths in the 3-5 and 5-8 μm size fraction, color coded according to cell size as shown in legend, where the regression between coccolith size and cell size (Henderiks, 2008) is employed. B) $\Delta_{cocco\text{-}DIC}$ vs $[CO_2]_{aq}$ for cultured *C. pelagicus* and *C. leptoporus* with color scale indicating DIC concentration (mM). Sources of culture data given in Table 1. C) Isotopic fractionation of sedimentary coccoliths during the latest Eocene and earliest Oligocene, comparing isotopic differences between large and small coccoliths, $\Delta^{13}C_{large\text{-}small}$ (black symbols) and $\Delta^{13}C_{large\text{-}DIC}$ (red symbols) during the latest Eocene and earliest Oligocene, using coccolith isotopic data from Tremblin et al (2017) and $\delta^{13}C$ of DIC estimated from benthic foraminifera and a constant benthic-planktic $\delta^{13}C$ gradient of 0.94 ‰ (Zhang et al., 2013). Also shown is Uk'37 based sea surface temperature estimation (green) from ODP 511 from (Liu et al., 2009). D) Comparison of $\Delta^{13}C_{large\text{-}small}$ (green) and $\Delta^{13}C_{large\text{-}foram}$ (orange symbols) for the late Miocene-Pliocene in the Western Tropical Atlantic at ODP 925 (from Bolton et al., 2016) and $\Delta^{13}C_{large\text{-}foram}$ from ODP 846 (turquoise symbols; foraminifera data from Mejia et al., 2017). For comparison, in black diamonds is shown a pCO_2 curve derived from diatom ε_p in the Equatorial Pacific (Mejia et al., 2017); the illustrated curve shows pCO_2 assuming diatom growth rates of 1 day^{-1}. Also shown are alkenone-based sea surface temperatures from ODP Site 1088 (Herbert et al., 2016). $[CO_2]_{aq}$ in μM.

References

Andersen, N., Müller, P., Kirst, G., Schneider, R., 1999. Alkenone δ 13 C as a Proxy for PastPCO 2 in Surface Waters: Results from the Late Quaternary Angola Current, Use of Proxies in Paleoceanography. Springer, pp. 469-488.

Bach, L.T., Mackinder, L., Schulz, K.G., Wheeler, G., Schroeder, D.C., Brownlee, C., Riebesell, U., 2013. Dissecting the impact of CO2 and pH on the mechanisms of photosynthesis and calcification in the coccolithophore Emiliania huxleyi. New Phytologist 199, 121-134.

Bassinot, F., Marzin, C., Braconnot, P., Marti, O., Mathien-Blard, E., Lombard, F., Bopp, L., 2011. Holocene evolution of summer winds and marine productivity in the tropical Indian Ocean in response to insolation forcing: data-model comparison. Climate of the Past 7, 815-829.

Beaufort, L., 2007. Precession and ENSO-like variability in the Equatorial Indo-Pacific Ocean. Elsevier Oceanography Series 73, 273-294.

Beaufort, L., Couapel, M., Buchet, N., Claustre, H., Goyet, C., 2008. Calcite production by coccolithophores in the south east Pacific Ocean. Biogeosciences 5, 1101-1117.

Beaufort, L., Probert, I., De Garidel-Thoron, T., Bendif, E.M., Ruiz-Pino, D., Metzl, N., Goyet, C., Buchet, N., Coupel, P., Grelaud, M., 2011. Sensitivity of coccolithophores to carbonate chemistry and ocean acidification. Nature 476, 80.

Bidigare, R.R., Fluegge, A., Freeman, K.H., Hanson, K.L., Hayes, J.M., Hollander, D., Jasper, J.P., King, L.L., Laws, E.A., Milder, J., 1997. Consistent fractionation of 13C in nature and in the laboratory: Growth-rate effects in some haptophyte algae. Global Biogeochemical Cycles 11, 279-292.

Birch, H., Coxall, H.K., Pearson, P.N., Kroon, D., O'Regan, M., 2013. Planktonic foraminifera stable isotopes and water column structure: Disentangling ecological signals. Marine Micropaleontology 101, 127-145.

Bollmann, J., 1997. Morphology and biogeography of Gephyrocapsa coccoliths in Holocene sediments. Marine Micropaleontology 29, 319-350.

Bolton, C.T., Hernández-Sánchez, M.T., Fuertes, M.-Á., González-Lemos, S., Abrevaya, L., Mendez-Vicente, A., Flores, J.-A., Probert, I., Giosan, L., Johnson, J., 2016. Decrease in coccolithophore calcification and CO2 since the middle Miocene. Nature communications 7.

Bolton, C.T., Stoll, H.M., 2013. Late Miocene threshold response of marine algae to carbon dioxide limitation. Nature 500, 558-562.

Cassar, N., Laws, E.A., Popp, B.N., 2006. Carbon isotopic fractionation by the marine diatom Phaeodactylum tricornutum under nutrient-and light-limited growth conditions. Geochimica et cosmochimica acta 70, 5323-5335.

Endeward, V., Al-Samir, S., Itel, F., Gros, G., 2014. How does carbon dioxide permeate cell membranes? A discussion of concepts, results and methods. Frontiers in physiology 4, 382.

Feng, Y., Roleda, M.Y., Armstrong, E., Boyd, P.W., Hurd, C.L., 2017. Environmental controls on the growth, photosynthetic and calcification rates of a Southern Hemisphere strain of the coccolithophore Emiliania huxleyi. Limnology and Oceanography 62, 519-540.

Fielding, S.R., 2013. Emiliania huxleyi specific growth rate dependence on temperature. Limnology and Oceanography 58, 663-666.

Francois, R., Altabet, M.A., Goericke, R., McCorkle, D.C., Brunet, C., Poisson, A., 1993. Changes in the δ13C of surface water particulate organic matter across the subtropical convergence in the SW Indian Ocean. Global Biogeochemical Cycles 7, 627-644.

Goericke, R., Fry, B., 1994. Variations of marine plankton δ13C with latitude, temperature, and dissolved CO2 in the world ocean. J Global Biogeochemical Cycles 8, 85-90.

Hain, M.P., Sigman, D.M., Higgins, J.A., Haug, G.H., 2015. The effects of secular calcium and magnesium concentration changes on the thermodynamics of seawater acid/base chemistry: Implications for Eocene and Cretaceous ocean carbon chemistry and buffering. Global Biogeochemical Cycles 29, 517-533.
Henderiks, J., 2008. Coccolithophore size rules—Reconstructing ancient cell geometry and cellular calcite quota from fossil coccoliths. Marine Micropaleontology 67, 143-154.
Henderiks, J., Pagani, M., 2008. Coccolithophore cell size and the Paleogene decline in atmospheric CO 2. Earth and Planetary Science Letters 269, 576-584.
Herbert, T.D., Lawrence, K.T., Tzanova, A., Peterson, L.C., Caballero-Gill, R., Kelly, C.S., 2016. Late Miocene global cooling and the rise of modern ecosystems. Nature Geoscience 9, 843–847
Hermoso, M., 2016. Isotopic record of Pleistocene glacial/interglacial cycles in pelagic carbonates: Revisiting historical data from the Caribbean Sea. Quaternary Science Reviews 137, 69-78.
Hermoso, M., Chan, I., McClelland, H., Heureux, A., Rickaby, R., 2016. Vanishing coccolith vital effects with alleviated carbon limitation. Biogeosciences 13, 301.
Hernandez-Almeida, I., 2018. Core top calibration of sediment proxy indicators to phytoplankton growth rate for improving past CO2 estimates, 10th International Carbon Dioxide Conference, Interlaken.
Heureux, A.M., Rickaby, R.E., 2015. Refining our estimate of atmospheric CO 2 across the Eocene–Oligocene climatic transition. Earth and Planetary Science Letters 409, 329-338.
Hoins, M., Eberlein, T., Van de Waal, D.B., Sluijs, A., Reichart, G.-J., Rost, B., ecology, 2016. CO2-dependent carbon isotope fractionation in dinoflagellates relates to their inorganic carbon fluxes. Journal of experimental marine biology 481, 9-14.
Holmes, M.E., Schneider, R.R., Müller, P.J., Segl, M., Wefer, G., 1997. Reconstruction of past nutrient utilization in the eastern Angola Basin based on sedimentary 15N/14N ratios. Paleoceanography 12, 604-614.
Holtz, L.-M., Wolf-Gladrow, D., Thoms, S., 2015. Numerical cell model investigating cellular carbon fluxes in Emiliania huxleyi. Journal of theoretical biology 364, 305-315.
Holtz, L.-M., Wolf-Gladrow, D., Thoms, S., 2017. Stable carbon isotope signals in particulate organic and inorganic carbon of coccolithophores–A numerical model study for Emiliania huxleyi. Journal of Theoretical Biology 420, 117-127.
Hopkinson, B.M., 2014. A chloroplast pump model for the CO2 concentrating mechanism in the diatom Phaeodactylum tricornutum. Photosynthesis research 121, 223-233.
Hopkinson, B.M., Dupont, C.L., Allen, A.E., Morel, F.M., 2011. Efficiency of the CO2-concentrating mechanism of diatoms. Proceedings of the National Academy of Sciences 108, 3830-3837.
Itel, F., Al-Samir, S., Öberg, F., Chami, M., Kumar, M., Supuran, C.T., Deen, P.M., Meier, W., Hedfalk, K., Gros, G., 2012. CO2 permeability of cell membranes is regulated by membrane cholesterol and protein gas channels. The FASEB Journal 26, 5182-5191.
Ivanochko, T.S., Ganeshram, R.S., Brummer, G.-J.A., Ganssen, G., Jung, S.J., Moreton, S.G., Kroon, D., 2005. Variations in tropical convection as an amplifier of global climate change at the millennial scale. Earth and Planetary Science Letters 235, 302-314.
Jasper, J.P., Hayes, J., Mix, A.C., Prahl, F.G., 1994. Photosynthetic fractionation of 13C and concentrations of dissolved CO2 in the central equatorial Pacific during the last 255,000 years. Paleoceanography 9, 781-798.
Jones, B.M., Iglesias-Rodriguez, M.D., Skipp, P.J., Edwards, R.J., Greaves, M.J., Young, J.R., Elderfield, H., O'Connor, C.D., 2013. Responses of the Emiliania huxleyi proteome to ocean acidification. PloS One 8, e61868.
Kai, L., Kaldenhoff, R., 2014. A refined model of water and CO 2 membrane diffusion: Effects and contribution of sterols and proteins. Scientific reports 4, 6665.
Keller, K., Morel, F.M., 1999. A model of carbon isotopic fractionation and active carbon uptake in phytoplankton. Marine Ecology Progress Series 182, 295-298.
Kottmeier, D.M., Rokitta, S.D., Rost, B., 2016. H+-driven increase in CO2 uptake and decrease in HCO3− uptake explain coccolithophores' acclimation responses to ocean acidification. Limnology and Oceanography 61, 2045-2057.

Kottmeier, D.M., Rokitta, S.D., Tortell, P.D., Rost, B., 2014. Strong shift from HCO3− to CO2 uptake in Emiliania huxleyi with acidification: new approach unravels acclimation versus short-term pH effects. Photosynthesis research 121, 265-275.
Kranz, S.A., Young, J.N., Hopkinson, B.M., Goldman, J.A., Tortell, P.D., Morel, F.M., 2015. Low temperature reduces the energetic requirement for the CO2 concentrating mechanism in diatoms. New Phytologist 205, 192-201.
Krumhardt, K.M., Lovenduski, N.S., Iglesias-Rodriguez, M.D., Kleypas, J.A., 2017. Coccolithophore growth and calcification in a changing ocean. Progress in Oceanography 159, 276-295.
Laws, E.A., Popp, B.N., Bidigare, R.R., Riebesell, U., Burkhardt, S., Wakeham, S.G., 2001. Controls on the molecular distribution and carbon isotopic composition of alkenones in certain haptophyte algae. Geochemistry, Geophysics, Geosystems 2.
Liu, Z., Pagani, M., Zinniker, D., DeConto, R., Huber, M., Brinkhuis, H., Shah, S.R., Leckie, R.M., Pearson, A., 2009. Global cooling during the Eocene-Oligocene climate transition. Science 323, 1187-1190.
McClelland, H., Bruggeman, J., Hermoso, M., Rickaby, R., 2017. The origin of carbon isotope vital effects in coccolith calcite. Nature Communications 8.
Mejia, L.M., Mendez-Vicente, A., Abrevaya, L., Lawrence, K., Ladlow, C., Bolton, C., Cacho, I., Stoll, H., 2017. A diatom record of CO2 decline since the late Miocene. Earth and Planetary Science Letters 479, 18-33.
Mejía, L.M., Ziveri, P., Cagnetti, M., Bolton, C., Zahn, R., Marino, G., Martínez-Méndez, G., Stoll, H., 2014. Effects of midlatitude westerlies on the paleoproductivity at the Agulhas Bank slope during the penultimate glacial cycle: Evidence from coccolith Sr/Ca ratios. Paleoceanography and Paleoclimatology 29, 697-714.
Meyer, M., Griffiths, H., 2013. Origins and diversity of eukaryotic CO2-concentrating mechanisms: lessons for the future. Journal of experimental botany 64, 769-786.
Molfino, B., McIntyre, A., 1990. Precessional forcing of nutricline dynamics in the equatorial Atlantic. Science 249, 766.
Monteiro, F.M., Bach, L.T., Brownlee, C., Bown, P., Rickaby, R.E., Poulton, A.J., Tyrrell, T., Beaufort, L., Dutkiewicz, S., Gibbs, S., 2016. Why marine phytoplankton calcify. Science advances 2, e1501822.
Pagani, M., 2014. 12.13 Biomarker-Based Inferences of Past Climate: The Alkenone pCO2 Proxy. Treatise on Geochemistry. Elsevier, Oxford, 361-378.
Pagani, M., Huber, M., Liu, Z., Bohaty, S.M., Henderiks, J., Sijp, W., Krishnan, S., DeConto, R.M., 2011. The role of carbon dioxide during the onset of Antarctic glaciation. Science 334, 1261-1264.
Palmer, M., Brummer, G., Cooper, M., Elderfield, H., Greaves, M., Reichart, G., Schouten, S., Yu, J., 2010. Multi-proxy reconstruction of surface water pCO 2 in the northern Arabian Sea since 29ka. Earth and Planetary Science Letters 295, 49-57.
Petit, J.-R., Jouzel, J., Raynaud, D., Barkov, N.I., Barnola, J.-M., Basile, I., Bender, M., Chappellaz, J., Davis, M., Delaygue, G., 1999. Climate and atmospheric history of the past 420,000 years from the Vostok ice core, Antarctica. Nature 399, 429.
Popp, B.N., Kenig, F., Wakeham, S.G., Laws, E.A., Bidigare, R.R., 1998a. Does growth rate affect ketone unsaturation and intracellular carbon isotopic variability in Emiliania huxleyi?. Paleoceanography 13, 35–41.
Popp, B.N., Laws, E.A., Bidigare, R.R., Dore, J.E., Hanson, K.L., Wakeham, S.G., 1998b. Effect of phytoplankton cell geometry on carbon isotopic fractionation. Geochimica et cosmochimica acta 62, 69-77.
Rau, G., Riebesell, U., Wolf-Gladrow, D., 1996. A model of photosynthetic 13C fractionation by marine phytoplankton based on diffusive molecular CO2 uptake. Marine Ecology Progress Series 133, 275-285.
Rau, G., Riebesell, U., Wolf-Gladrow, D., 1997. CO2aq-dependent photosynthetic 13C fractionation in the ocean: A model versus measurements. Global Biogeochemical Cycles 11, 267-278.
Raven, J.A., Beardall, J., Giordano, M., 2014. Energy costs of carbon dioxide concentrating mechanisms in aquatic organisms. Photosynthesis Research 121, 111-124.

Reinfelder, J.R., 2010. Carbon concentrating mechanisms in eukaryotic marine phytoplankton. Annual Review of Marine Science 3, 291-315.
Rickaby, R.E., Henderiks, J., Young, J.N., 2010. Perturbing phytoplankton: a tale of isotopic fractionation in two coccolithophore species. Climate of the Past Discussions 6, 257-294.
Riebesell, U., Burkhardt, S., Dauelsberg, A., Kroon, B., 2000a. Carbon isotope fractionation by a marine diatom: dependence on the growth-rate-limiting resource. Marine Ecology Progress Series 193, 295-303.
Riebesell, U., Revill, A.T., Holdsworth, D.G., Volkman, J.K., 2000b. The effects of varying CO 2 concentration on lipid composition and carbon isotope fractionation in Emiliania huxleyi. Geochimica et Cosmochimica Acta 64, 4179-4192.
Rost, B., Zondervan, I., Riebesell, U., 2002. Light-dependent carbon isotope fractionation in the coccolithophorid Emiliania huxleyi. Limnology and Oceanography 47, 120-128.
Schulz, K.G., Rost, B., Burkhardt, S., Riebesell, U., Thoms, S., Wolf-Gladrow, D., 2007. The effect of iron availability on the regulation of inorganic carbon acquisition in the coccolithophore Emiliania huxleyi and the significance of cellular compartmentation for stable carbon isotope fractionation. Geochimica et Cosmochimica Acta 71, 5301-5312.
Seki, O., Foster, G.L., Schmidt, D.N., Mackensen, A., Kawamura, K., Pancost, R.D., 2010. Alkenone and boron-based Pliocene pCO 2 records. Earth and Planetary Science Letters 292, 201-211.
Sosdian, S., Greenop, R., Hain, M., Foster, G., Pearson, P., Lear, C., 2018. Constraining the evolution of Neogene ocean carbonate chemistry using the boron isotope pH proxy. Earth and Planetary Science Letters 498, 362-376.
Spero, H.J., Mielke, K.M., Kalve, E.M., Lea, D.W., Pak, D.K., 2003. Multispecies approach to reconstructing eastern equatorial Pacific thermocline hydrography during the past 360 kyr. Paleoceanography 18.
Stoll, H.M., 2005. Limited range of interspecific vital effects in coccolith stable isotopic records during the Paleocene-Eocene thermal maximum. Paleoceanography 20.
Stoll, H.M., Rosenthal, Y., Falkowski, P., 2002. Climate proxies from Sr/Ca of coccolith calcite: calibrations from continuous culture of Emiliania huxleyi. Geochimica et Cosmochimica Acta 66, 927-936.
Stoll, H.M., Ziveri, P., 2002. Separation of monospecific and restricted coccolith assemblages from sediments using differential settling velocity. Marine Micropaleontology 46, 209-221.
Tchernov, D., Gruber, D.F., Irwin, A., 2014. Isotopic fractionation of carbon in the coccolithophorid Emiliania huxleyi. Marine Ecology Progress Series 508, 53-66.
Tolosa, I., Miquel, J.-C., Gasser, B., Raimbault, P., Goyet, C., Claustre, H., 2008. Distribution of lipid biomarkers and carbon isotope fractionation in contrasting trophic environments of the South East Pacific. Biogeosciences 5, 949-968.
Tremblin, M., Hermoso, M., Minoletti, F., 2016. Equatorial heat accumulation as a long-term trigger of permanent Antarctic ice sheets during the Cenozoic. Proceedings of the National Academy of Sciences 113, 11782-11787.
Wang, Y., Stessman, D.J., Spalding, M.H., 2015. The CO 2 concentrating mechanism and photosynthetic carbon assimilation in limiting CO 2: how Chlamydomonas works against the gradient. The Plant Journal 82, 429-448.
Wilkes, E.B., Carter, S.J., Pearson, A., 2017. CO2-dependent carbon isotope fractionation in the dinoflagellate Alexandrium tamarense. Geochimica et Cosmochimica Acta 212, 48-61.
Wilkes E. B., Lee R. B. Y., McClelland H. L. O., Rickaby R. E. M., and Pearson A. (2018) Carbon isotope ratios of coccolith-associated polysaccharides as a function of growth rate and CO2 concentration. *Organic Geochemistry* **119**, 1-10.
Zeebe, R.E., 2012. History of seawater carbonate chemistry, atmospheric CO2, and ocean acidification. Annual Review of Earth and Planetary Sciences 40, 141-165.
Zhang, Y.G., Pagani, M., Liu, Z., Bohaty, S.M., DeConto, R., 2013. A 40-million-year history of atmospheric CO2. Phil. Trans. R. Soc. A 371, 20130096.
Ziveri, P., Stoll, H., Probert, I., Klaas, C., Geisen, M., Ganssen, G., Young, J., 2003. Stable isotope 'vital effects' in coccolith calcite. Earth and Planetary Science Letters 210, 137-149.

384

385

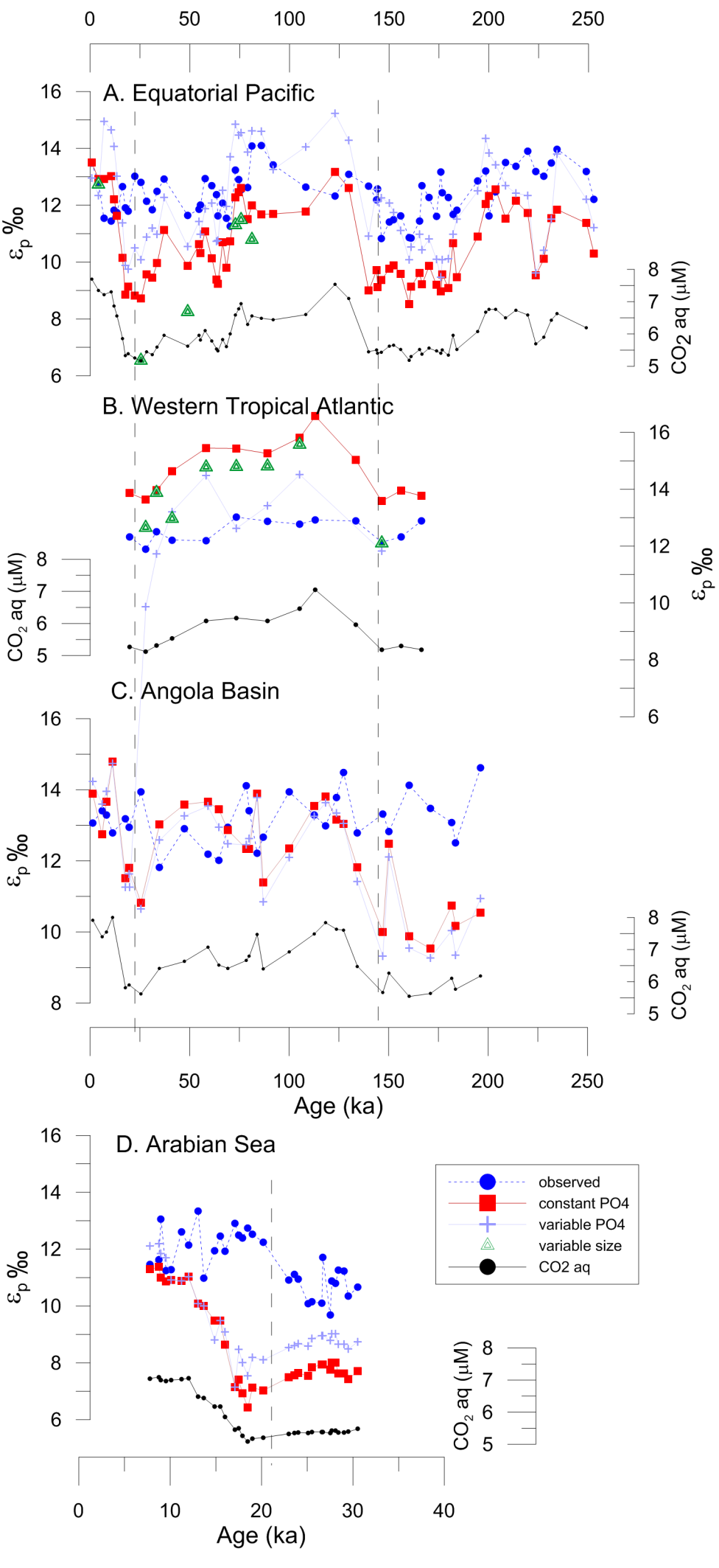
A. Equatorial Pacific
B. Western Tropical Atlantic
C. Angola Basin
D. Arabian Sea
εp ‰
CO2 aq (µM)
Age (ka)
observed
constant PO4
variable PO4
variable size
CO2 aq

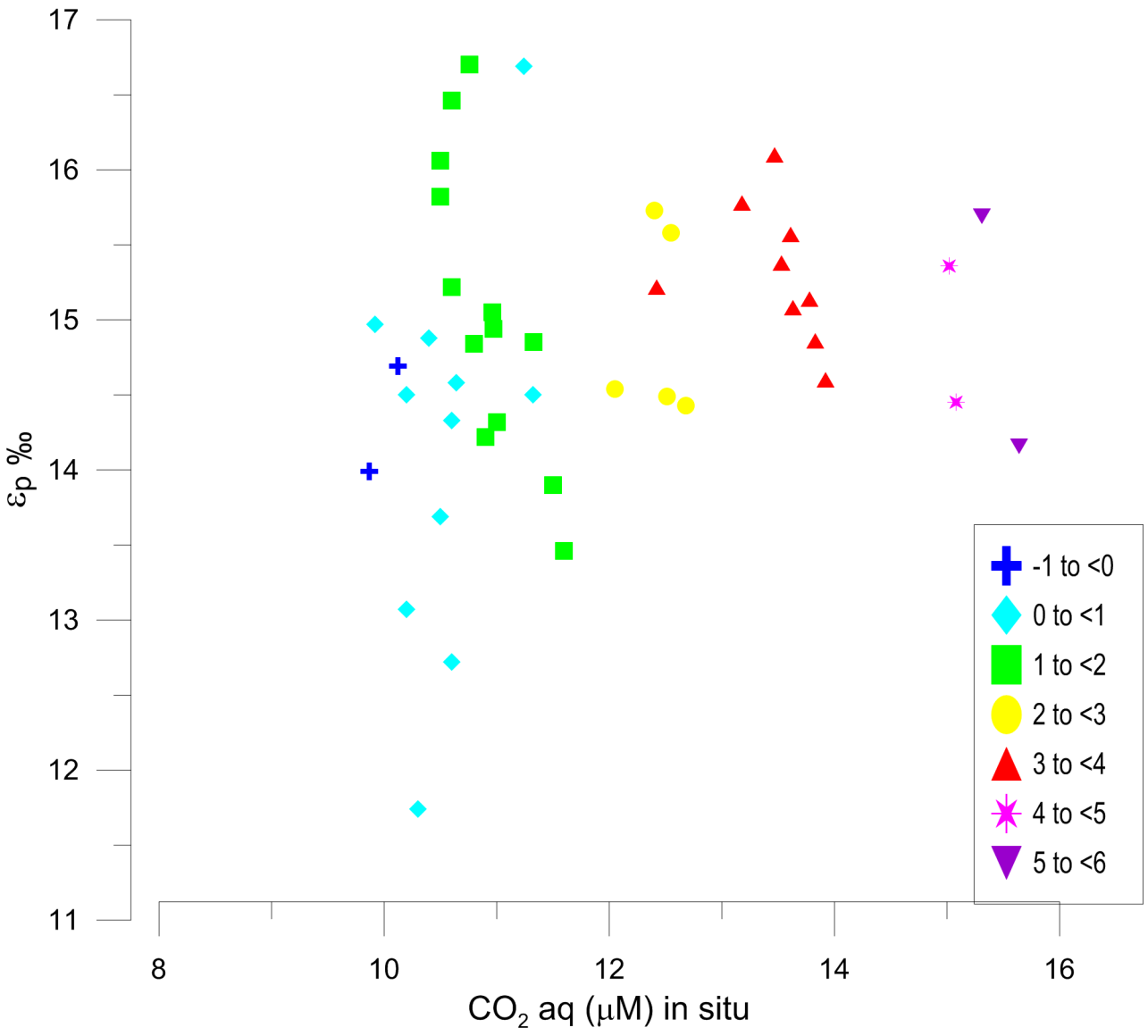
17
16
15
14
13
12
11
εp ‰
8
10
12
14
16
CO2 aq (μM) in situ
-1 to <0
0 to <1
1 to <2
2 to <3
3 to <4
4 to <5
5 to <6

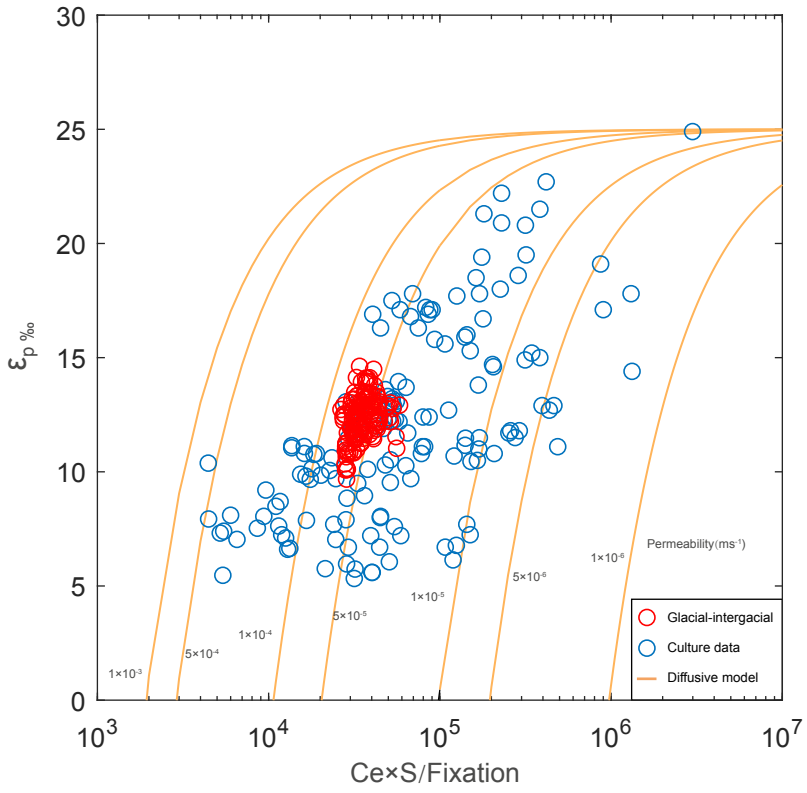
30
25
20
15
10
5
0
ε_p ‰
10^3
10^4
10^5
10^6
10^7
Ce×S/Fixation
1×10⁻³
5×10⁻⁴
1×10⁻⁴
5×10⁻⁵
1×10⁻⁵
5×10⁻⁶
1×10⁻⁶
Permeability(ms⁻¹)
Glacial-intergacial
Culture data
Diffusive model

Figure 4

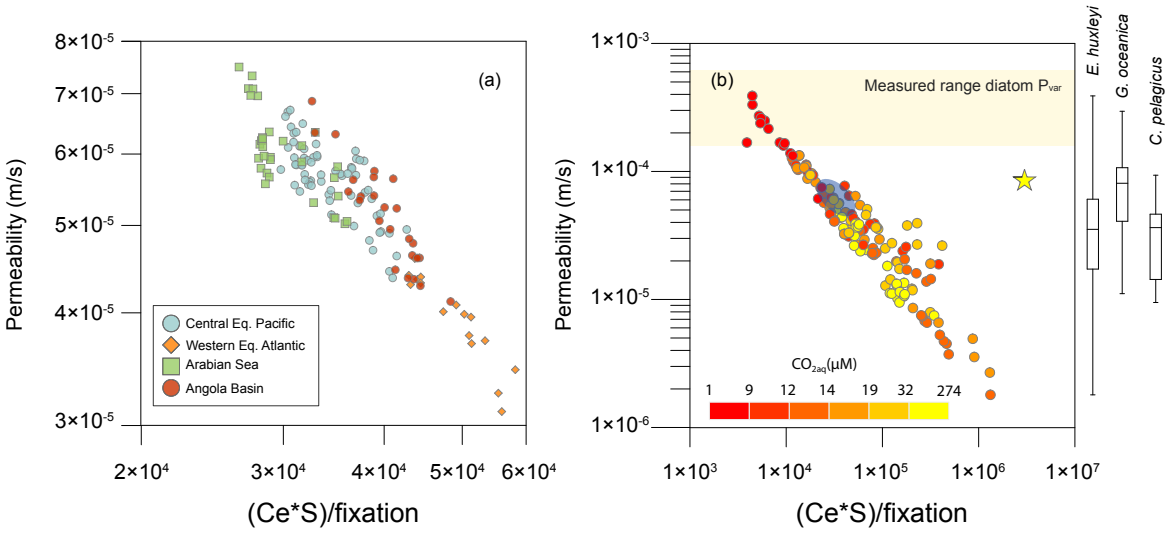
(a)
Permeability (m/s)
8×10-5
7×10-5
6×10-5
5×10-5
4×10-5
3×10-5
2×10⁴
3×10⁴
4×10⁴
5×10⁴
6×10⁴
(Ce*S)/fixation
Central Eq. Pacific
Western Eq. Atlantic
Arabian Sea
Angola Basin
(b)
Measured range diatom Pvar
Permeability (m/s)
1×10-3
1×10-4
1×10-5
1×10-6
1×10³
1×10⁴
1×10⁵
1×10⁶
1×10⁷
(Ce*S)/fixation
CO2aq(µM)
1
9
12
14
19
32
274
E. huxleyi
G. oceanica
C. pelagicus

Figure 5

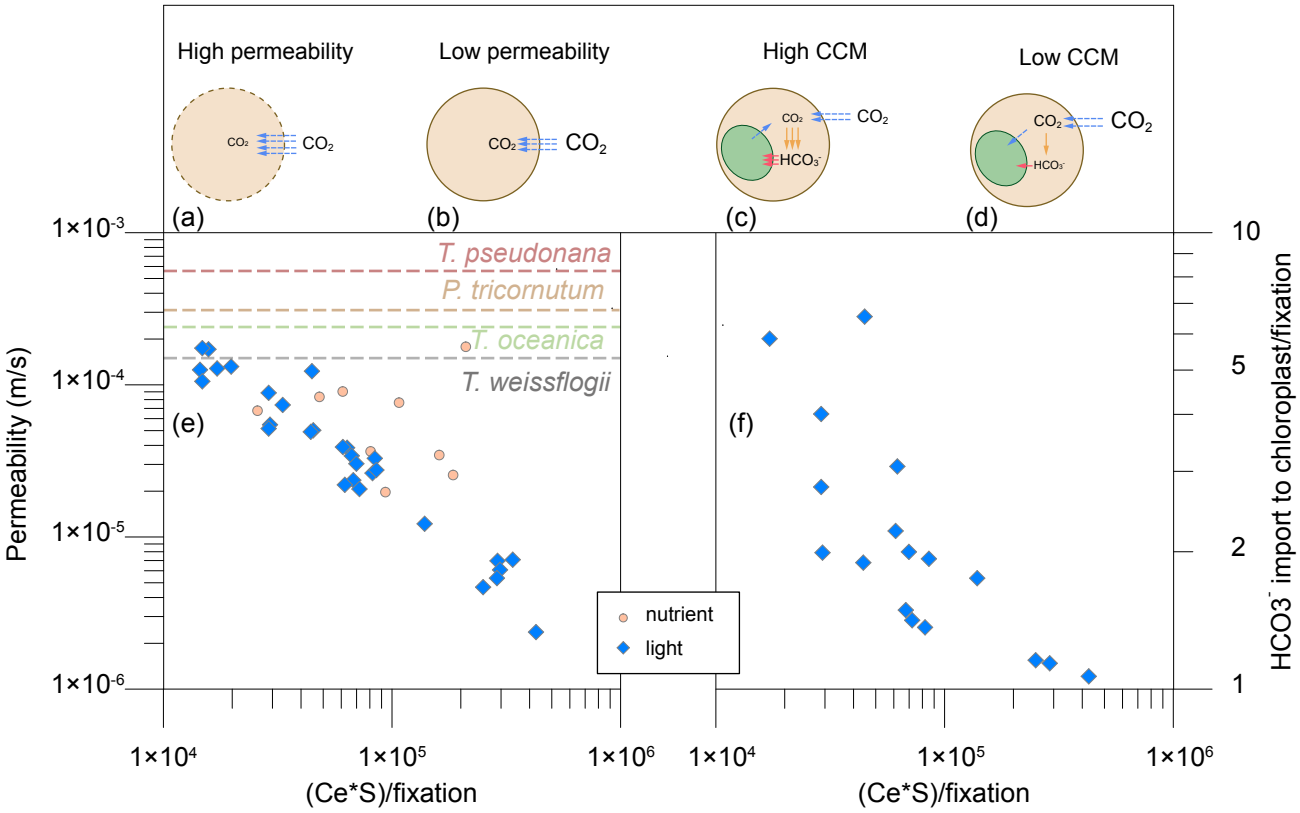
High permeability
Low permeability
High CCM
Low CCM
CO2
HCO3-
(a)
(b)
(c)
(d)
T. pseudonana
P. tricornutum
T. oceanica
T. weissflogii
(e)
(f)
nutrient
light
Permeability (m/s)
1×10-3
1×10-4
1×10-5
1×10-6
HCO3- import to chloroplast/fixation
10
5
2
1
1×10⁴
1×10⁵
1×10⁶
(Ce*S)/fixation

Figure 6

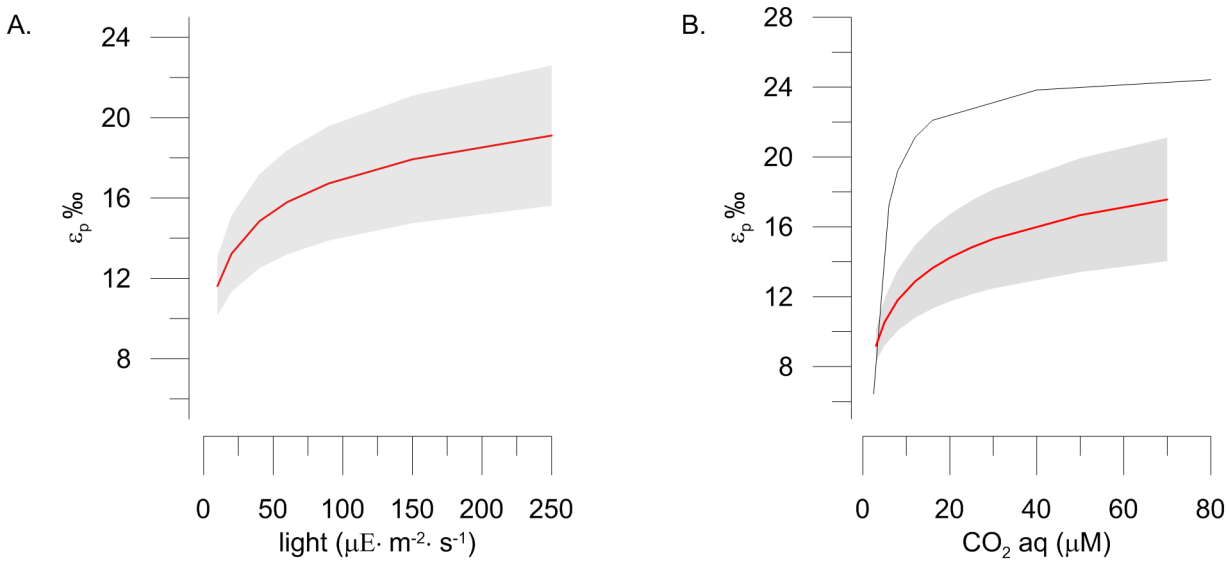
A.
24
20
16
12
8
ε_p ‰
0
50
100
150
200
250
light (μE· m^{-2}· s^{-1})
B.
28
24
20
16
12
8
ε_p ‰
0
20
40
60
80
CO_2 aq (μM)

Figure 7

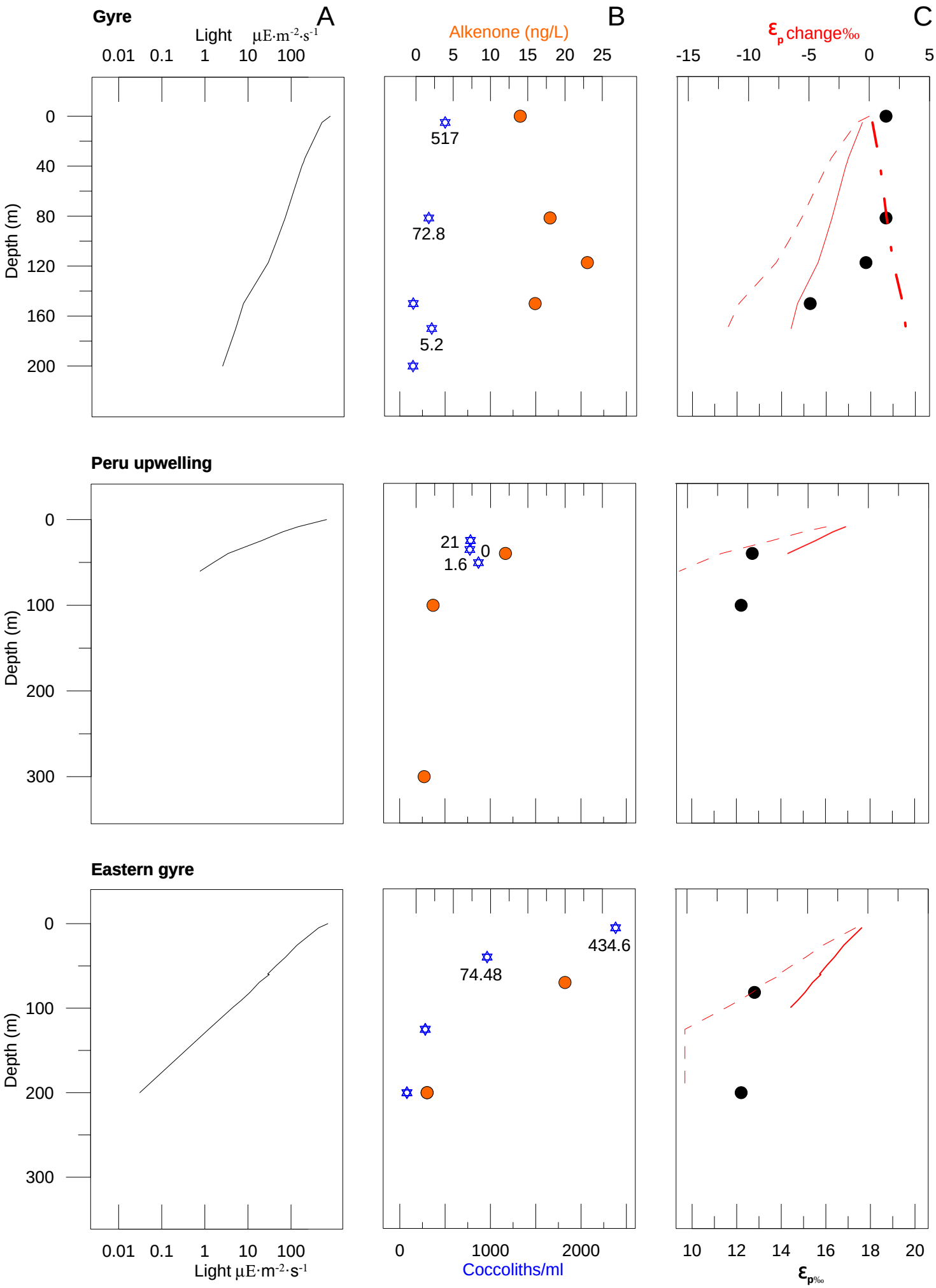
Gyre
A
Light μE·m-2·s-1
0.01 0.1 1 10 100
B
Alkenone (ng/L)
0 5 10 15 20 25
C
εp change‰
-15 -10 -5 0 5
Depth (m)
0 40 80 120 160 200
517
72.8
5.2
Peru upwelling
0 100 200 300
21
1.6
0
Eastern gyre
0 100 200 300
434.6
74.48
0.01 0.1 1 10 100
Light μE·m-2·s-1
0 1000 2000
Coccoliths/ml
10 12 14 16 18 20
εp‰

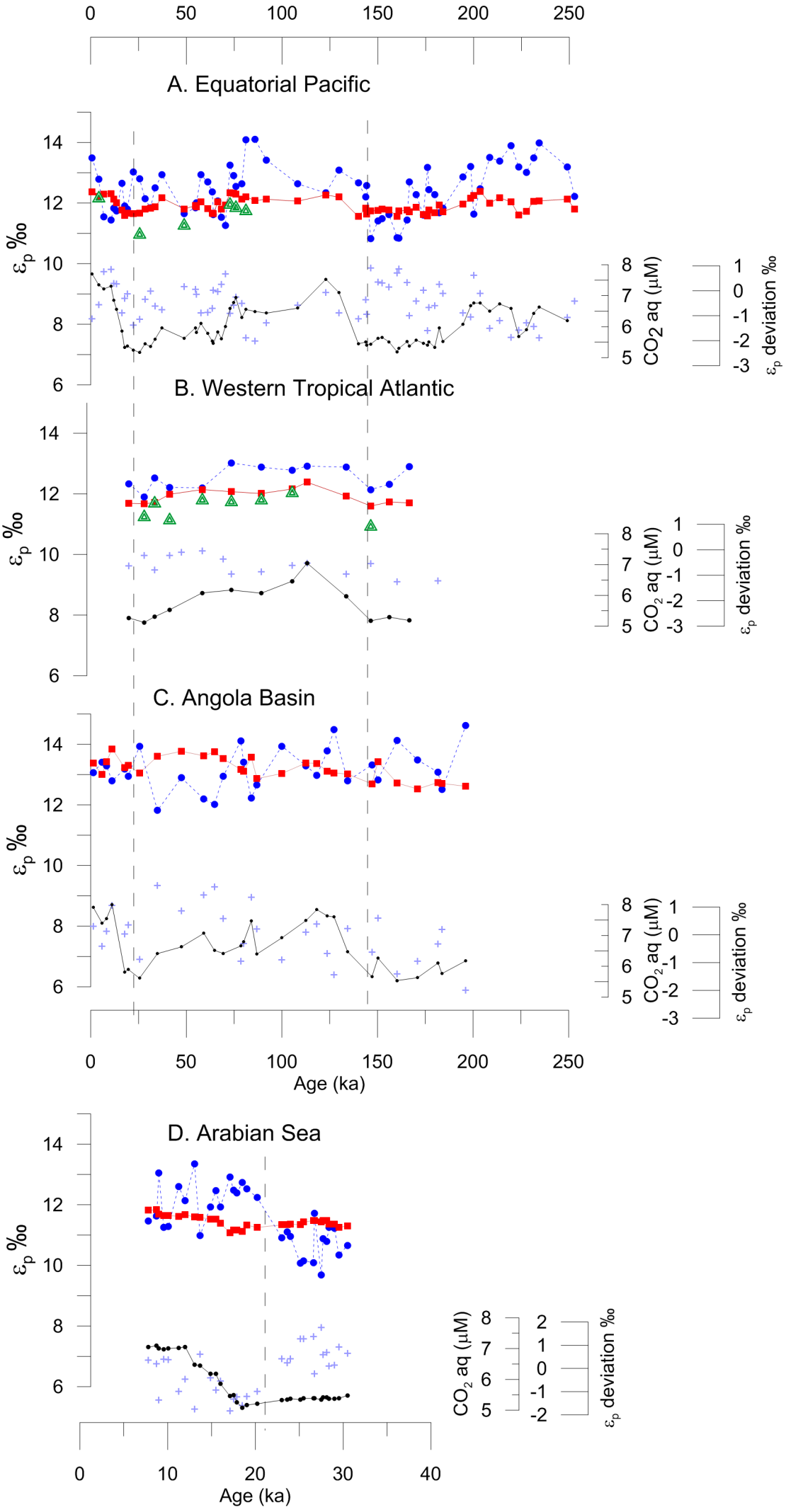
A. Equatorial Pacific
B. Western Tropical Atlantic
C. Angola Basin
D. Arabian Sea
εp ‰
CO2 aq (µM)
εp deviation ‰
Age (ka)

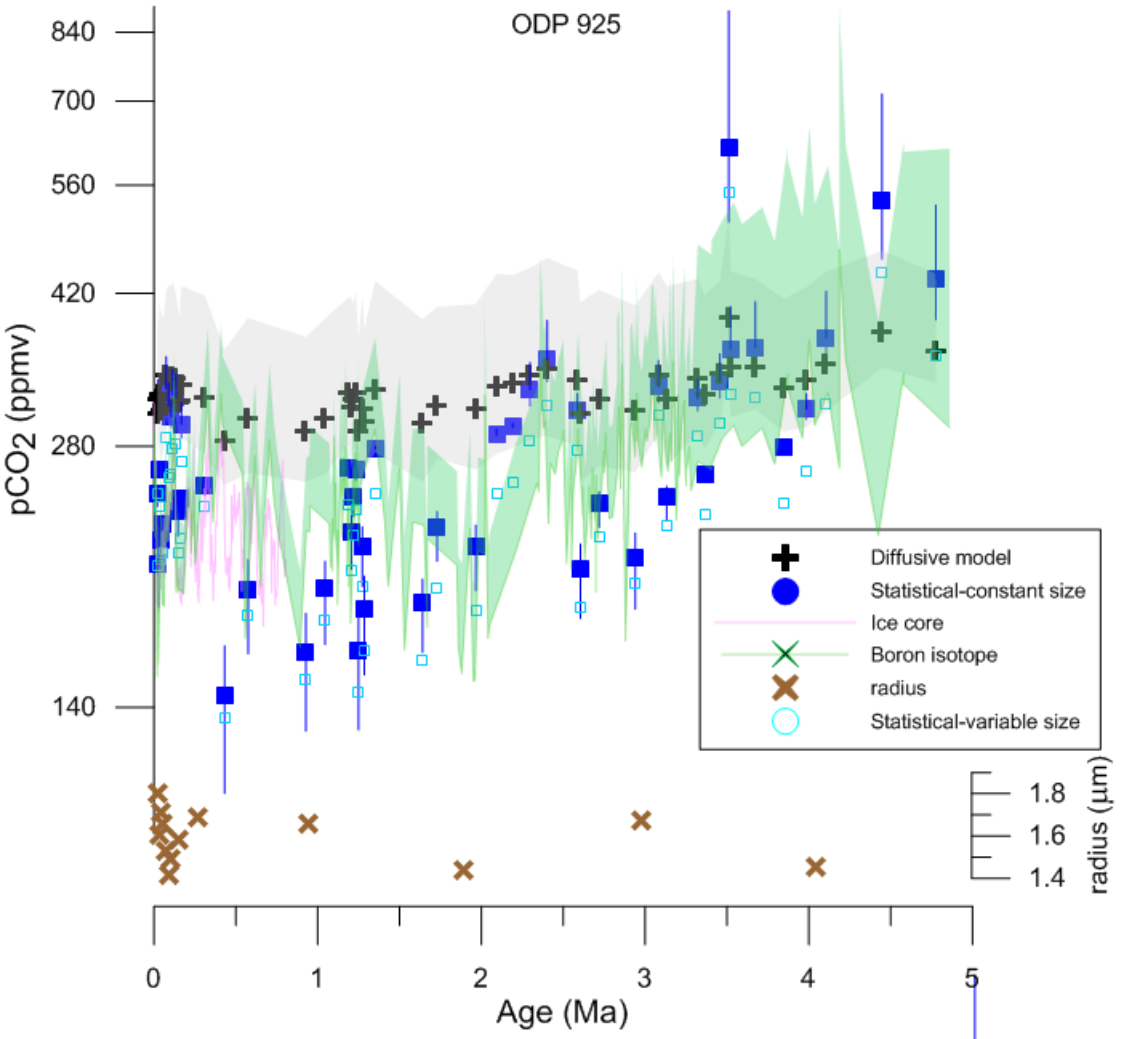
ODP 925
840
700
560
420
280
140
pCO2 (ppmv)
Diffusive model
Statistical-constant size
Ice core
Boron isotope
radius
Statistical-variable size
1.8
1.6
1.4
radius (µm)
0
1
2
3
4
5
Age (Ma)

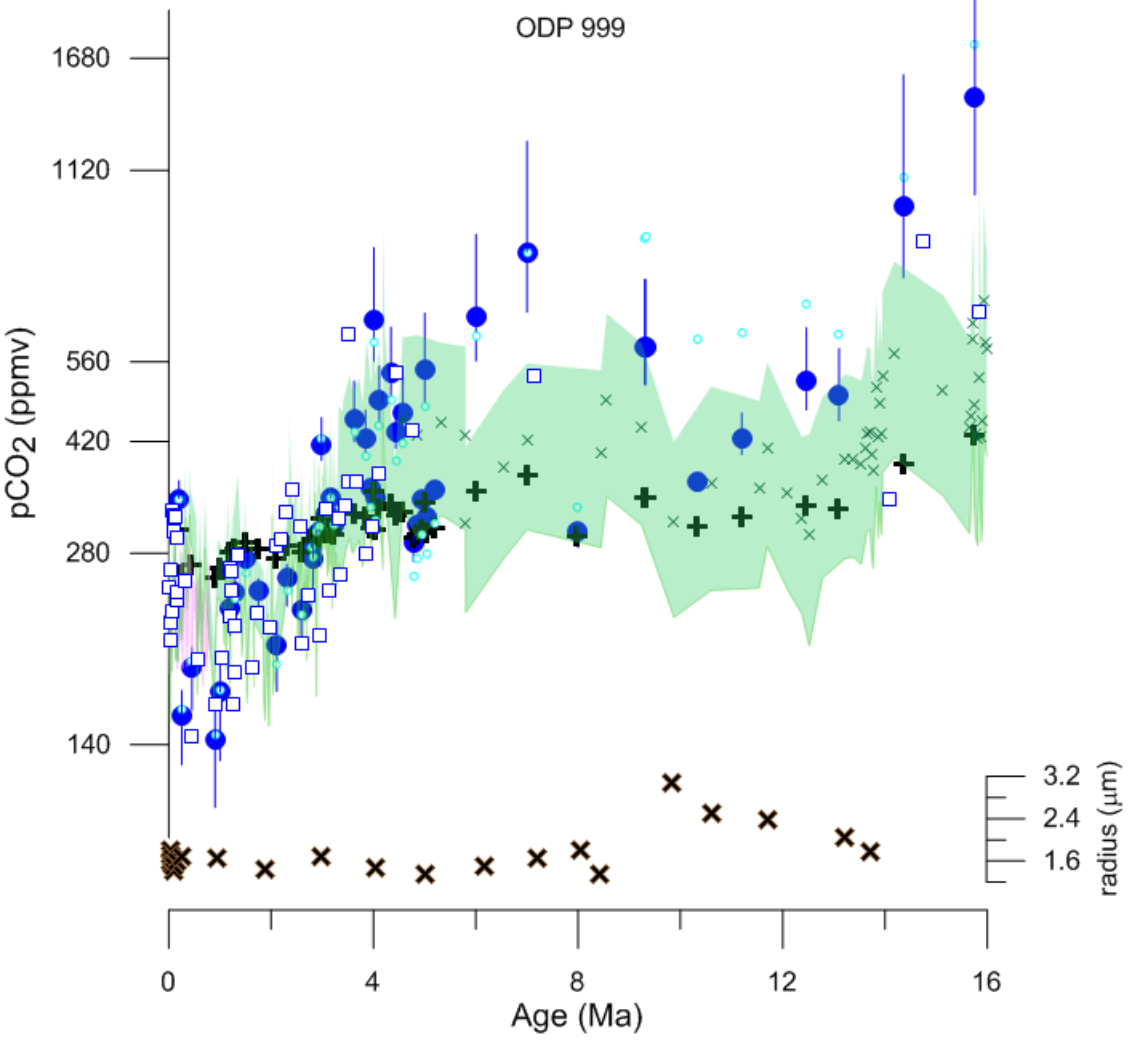
ODP 999
1680
1120
560
420
280
140
pCO2 (ppmv)
3.2
2.4
1.6
radius (µm)
0
4
8
12
16
Age (Ma)

Figure 10

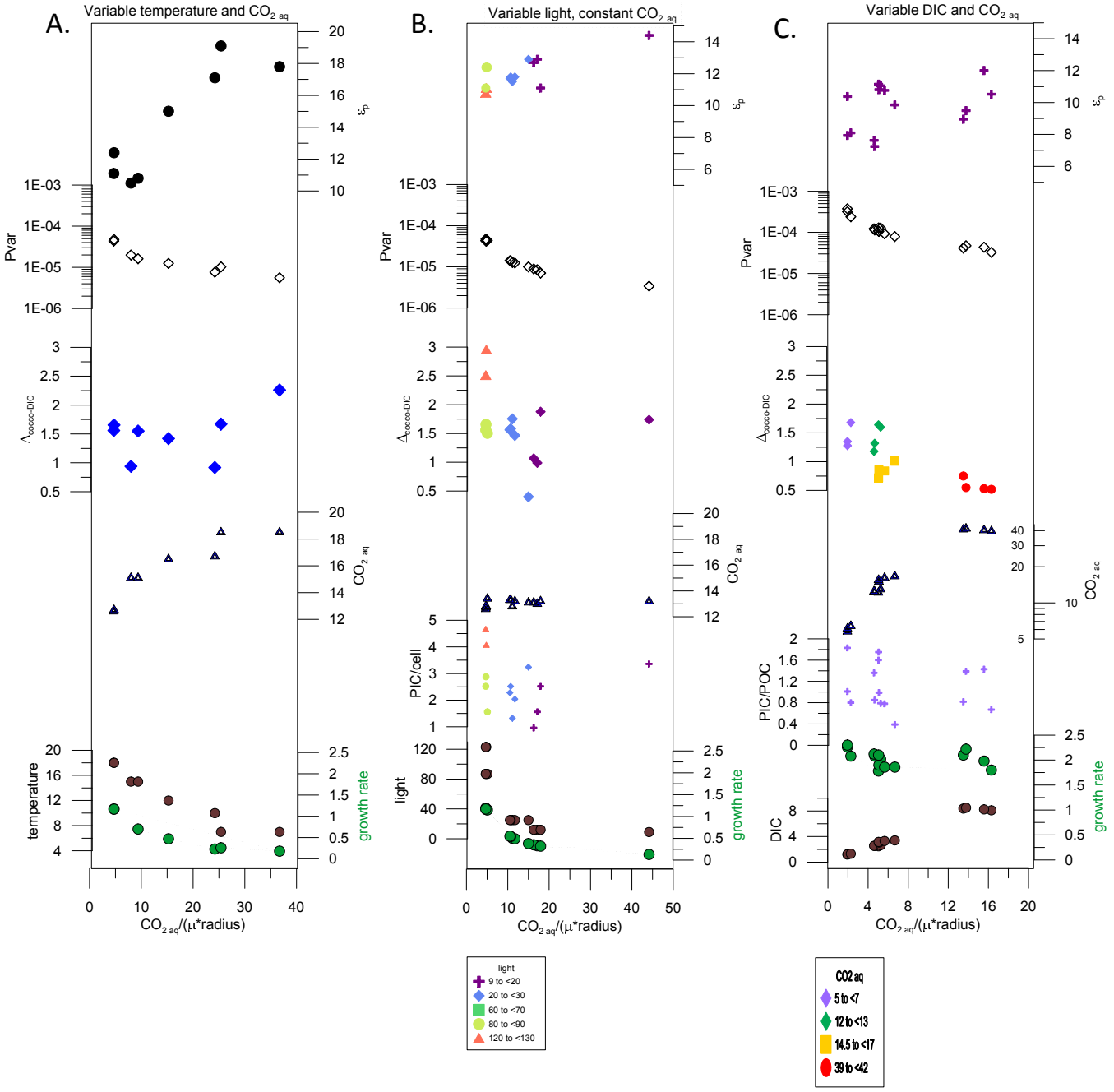
A.
Variable temperature and $CO_{2\ aq}$
B.
Variable light, constant $CO_{2\ aq}$
C.
Variable DIC and $CO_{2\ aq}$
Pvar
ε_p
$\Delta_{cocco-DIC}$
$CO_{2\ aq}$
temperature
growth rate
PIC/cell
light
PIC/POC
DIC
$CO_{2\ aq}/(\mu*radius)$
light
9 to <20
20 to <30
60 to <70
80 to <90
120 to <130
CO2 aq
5 to <7
12 to <13
14.5 to <17
39 to <42

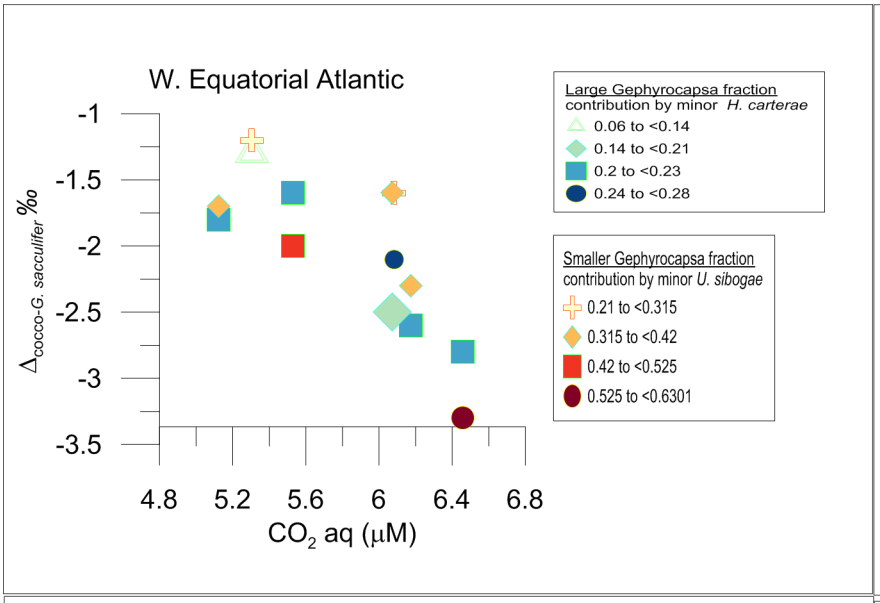
W. Equatorial Atlantic
Large Gephyrocapsa fraction
contribution by minor H. carterae
0.06 to <0.14
0.14 to <0.21
0.2 to <0.23
0.24 to <0.28
Smaller Gephyrocapsa fraction
contribution by minor U. sibogae
0.21 to <0.315
0.315 to <0.42
0.42 to <0.525
0.525 to <0.6301
Δcocco-G. sacculifer ‰
-1
-1.5
-2
-2.5
-3
-3.5
4.8
5.2
5.6
6
6.4
6.8
CO2 aq (µM)

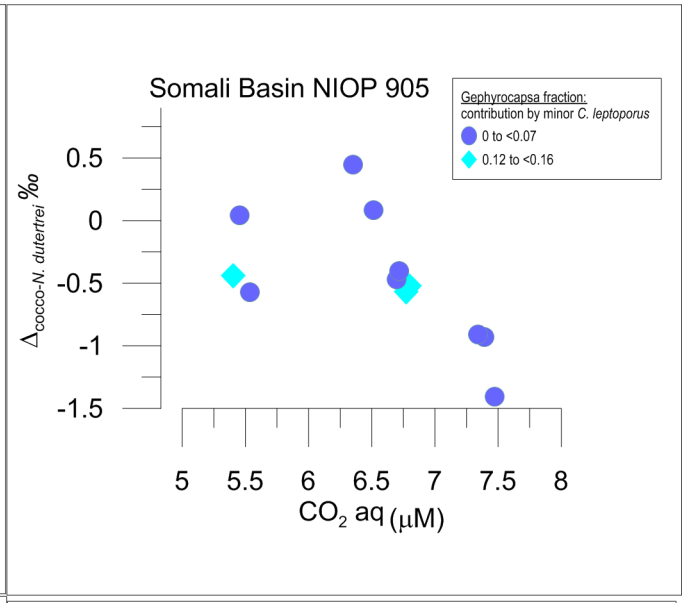
Somali Basin NIOP 905
Gephyrocapsa fraction:
contribution by minor C. leptoporus
0 to <0.07
0.12 to <0.16
Δcocco-N. dutertrei ‰
0.5
0
-0.5
-1
-1.5
5
5.5
6
6.5
7
7.5
8
CO2 aq (µM)

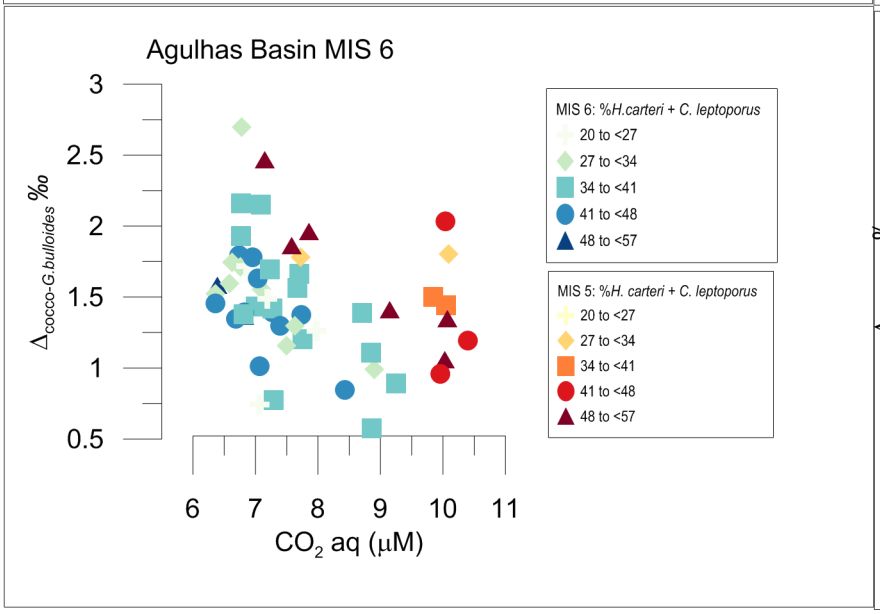
Agulhas Basin MIS 6
MIS 6: %H.carteri + C. leptoporus
20 to <27
27 to <34
34 to <41
41 to <48
48 to <57
MIS 5: %H. carteri + C. leptoporus
20 to <27
27 to <34
34 to <41
41 to <48
48 to <57
Δcocco-G.bulloides ‰
3
2.5
2
1.5
1
0.5
6
7
8
9
10
11
CO2 aq (µM)

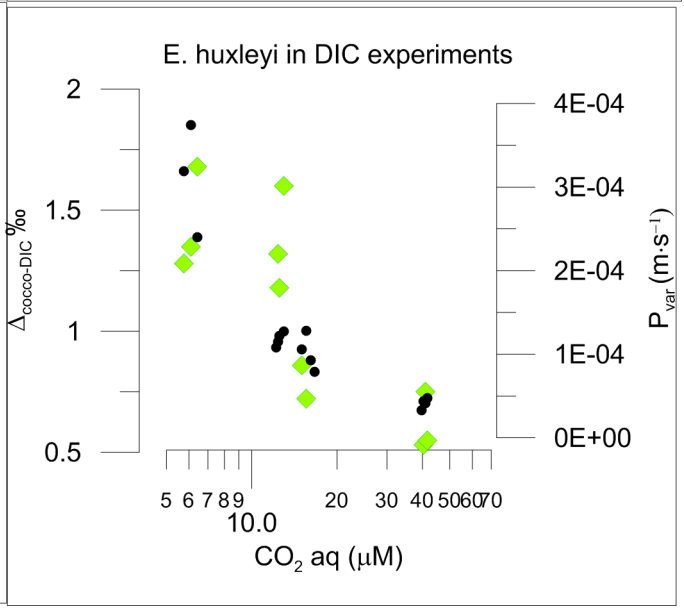
E. huxleyi in DIC experiments
Δcocco-DIC ‰
2
1.5
1
0.5
4E-04
3E-04
2E-04
1E-04
0E+00
Pvar (m·s-1)
5 6 7 8 9
10.0
20
30
40 50 60 70
CO2 aq (µM)

Figure 12

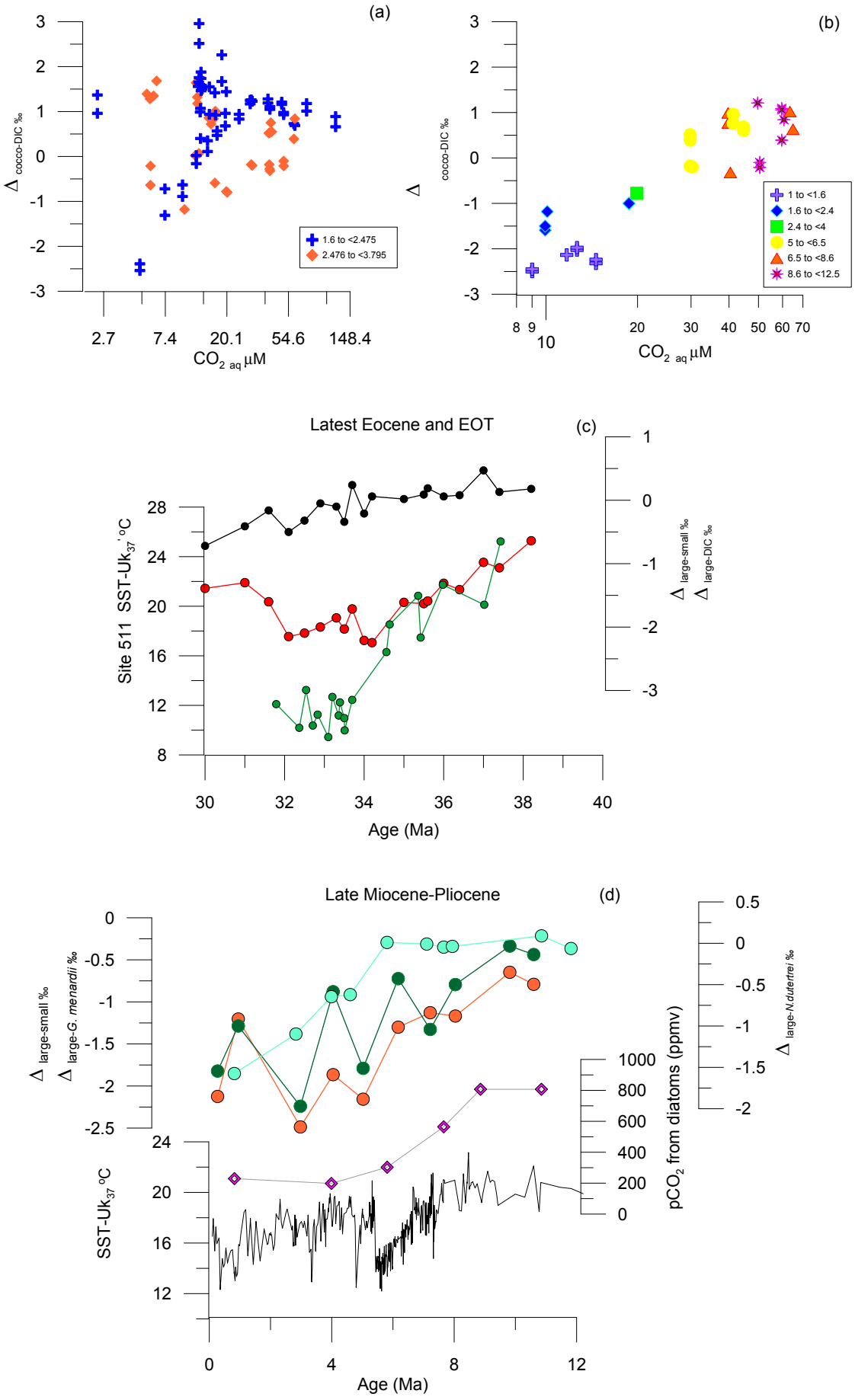
(a)
Δ cocco-DIC ‰
3
2
1
0
-1
-2
-3
1.6 to <2.475
2.476 to <3.795
2.7
7.4
20.1
54.6
148.4
CO2 aq µM
(b)
Δ cocco-DIC ‰
1 to <1.6
1.6 to <2.4
2.4 to <4
5 to <6.5
6.5 to <8.6
8.6 to <12.5
8 9 10 20 30 40 50 60 70
CO2 aq µM
Latest Eocene and EOT
(c)
Site 511 SST-UK37' °C
28
24
20
16
12
8
Δ large-small ‰
Δ large-DIC ‰
1
0
-1
-2
-3
30 32 34 36 38 40
Age (Ma)
Late Miocene-Pliocene
(d)
Δ large-small ‰
Δ large-G. menardii ‰
0
-0.5
-1
-1.5
-2
-2.5
SST-UK37 °C
24
20
16
12
pCO2 from diatoms (ppmv)
1000
800
600
400
200
0
Δ large-N.dutertrei ‰
0.5
0
-0.5
-1
-1.5
-2
0 4 8 12
Age (Ma)

Supplementary Methods for new data presented in this paper

Determination of % *Florisphaera profunda* in ODP 925

Smear slides for analyses of the relative abundance of *Florispahera profunda* were prepared following the methodology of Flores and Sierro (1997). A weight of 0.2 g of dry bulk sediment was diluted in 10 ml of buffered distilled water. The dilution was briefly sonicated in an ultrasonic bath, and then, 0.1 ml of the solution was pipetted out on a Petri-dish with a coverslip on its bottom. The Petri-dish had previously been filled with buffered distilled water and unflavoured gelatin to ensure homogenous distribution of the particles on the coverslip. After letting the particles settle overnight, the water was removed, the coverslip was dried at ambient temperature, and mounted with Canada Balsam on a slide. More than 400 coccoliths per sample were counted in a variable number of visual fields, using polarised-light microscopes at 1250× magnification. Relative abundance of *F. profunda* was calculated as a percentage of the total number of coccoliths.

Determinations of coccolith size in MANOP and ODP 925

Measurements of coccolith size was performed by processing microscopy images of sample slides prepared by the decantation method described in the previous section. A total of 20-25 fields of view were imaged by a Zeiss Axiocam 506 Color camera coupled to a Zeiss Axio Scope HAL100 POL microscope configured with circular polarized light and equipped with a Zeiss Plan-APOCHROMAT 100x/1.4 Oil objective. Coccolith length data was generated processing images with C-Calcita (Fuertes et al., 2014) and selecting an average of 200 individual alkenone producers' coccoliths.

Turbidostat culture determinations of Ecocco-DIC

New coccolith carbon isotope data here are reported for a series of turbidostat culture experiments first described in Stoll et al. (2001). Briefly, clonal cultures of *E. huxleyi* strain CCMP 374 were grown in nutrient-replete continuous cultures in a turbidostat system with 24 hour illumination at Rutgers University Institute of Marine and Coastal Sciences. The turbidostat system provided continuous culture dilution as a function of culture growth rate, to maintain constant media chemistry and cell densities around $3 \pm 0.5 \times 10^5$ cells/ml. Measured light intensities ranged from 9 to 146 $\mu Em^{-2}\ s^{-1}$ and temperatures ranged from 7 to 25° C. Media was prepared from New Jersey coastal seawater and nutrients enriched to f/50 or f/2 levels of Guillard (1975). The culture was bubbled continuously with air pumped from an intake outside of the laboratory building and pCO_2 in the culture chamber was measured

continuously using a LICOR monitoring system (Rosenthal et al., 1999). The strains were pre-adapted to experimental conditions for approximately 6 generation periods before collection of samples or growth rate data.

Cells were harvested after 6 generations at experimental conditions. Samples of culture media were filtered at 0.45 micron, preserved with HgCl, and stored in flame-sealed ampoules for determination of d13C of DIC as described in Tchernov et al. 2014. For isotope measurements in coccolith calcite, 360 ml of culture were centrifuged to form a pellet, the pellet was resuspended and cells were lysed using a sonication probe. The pellet was rinsed 8 times with distilled water buffered to pH 8 with addition of NaOH. Subsequently, the pellets were oxidized for 1 hour at 60° C in 500 µl of weak peroxide solution (0.35%) in 0.1M NaOH, and rinsed thoroughly with distilled water.

Stable carbon isotopes were determined on dried samples by samples were analyzed on a Fisons Optima mass spectrometer at the University of California, Santa Cruz with a reproducibility of 0.05 permil for $\delta^{13}C$.

Separation of coccolith in ODP 925 and NIOP 905 and

Coccolith size separation in samples from cores ODP 925 was performed by settling method following Stoll and Ziveri (2002), and using the settling velocities of different coccolith species determined by Zhang et al. (2018). A weight of 0.2 g of dry bulk sediment was suspended in 2% ammonium solution. Particles larger than 63 µm were removed by sieving. After sieving, the suspension was removed into a 50 ml centrifuge tube and added ammonium solution to 45 ml. The finest part including F. profunda and part of E. huxleyi and small Geophyrocapsa was removed by sinking for 5.5 h and removing the upper 30 ml suspension repeated by 6-8 times. Then the residue was added ammonium solution to 45 ml again and then settled for 2.7 h. The upper 30 ml suspension was pumped out, which contains the coccolith ranging from 3-5 µm. This fraction was dominated by the alkenone producer Geophyrocapa spp. (usually more than 80% in number), which was used for εcoccolith analyses in later step. Samples were rinsed at least 3 times in ultrapure MilliQ water and oven-dried at 50°C for several days. For NIOP 905, the samples were micro filtered to 3-5 and 5-8 µm fractions. Carbon isotope ratios on different size samples from both sediment cores were determined on dried samples at the Geological Institute of ETH Zurich on a ThermoFisher Delta V with GasBench II with a reproducibility of 0.05‰ permil for $\delta^{13}C$.

References

Flores, J. A., and Sierro, F. J. Revised technique for calculation of calcareous nannofossil accumulation rates. Micropaleontology, 1997, 43(3): 321-324.

Fuertes, M. Á., Flores, J. A., and Sierro, F. J. The use of circularly polarized light for biometry, identification and estimation of mass of coccoliths, Marine Micropaleontology, 2014, 113: 44–55.

Stoll H M, Ziveri P. Separation of monospecific and restricted coccolith assemblages from sediments using differential settling velocity. Marine Micropaleontology, 2002, 46(1-2): 209-221.

Stoll, H. M., Ruiz Encinar, J., Ignacio Garcia Alonso, J., Rosenthal, Y., Probert, I., & Klaas, C. A first look at paleotemperature prospects from Mg in coccolith carbonate: cleaning techniques and culture measurements. Geochemistry, Geophysics, Geosystems, 2001, 2(5).

Zhang, H., Stoll, H., Bolton, C., Jin, X., & Liu, C. A refinement of coccolith separation methods: measuring the sinking characteristics of coccoliths. Biogeosciences, 15(15), 4759-4775.

Supplementary figure and table captions

Figure S1: Map showing sediment core locations used in this study and modern surface ocean aqueous CO_2, in micromolar concentrations (μmol kg^{-1}). The map was generated using Ocean Data View (ODV) (Schlitzer, 2007) and the GLODAPv2 Bottle dataset (cdiac.ornl.gov/oceans/). Aqueous CO_2 concentrations were calculated using the built-in ODV ocean calculator with reported sea surface temperatures, pressures, alkalinity, and total dissolved inorganic carbon. The data were gridded using DIVA gridding with a 25 per mile scale length in the X and Y direction.

Figure S2: Variations in proxy indicators of growth rate at each of the four sites covering glacial-interglacial cycles.

Figure S3: Correlation table of variables in culture experiments listed in Table 1.

Figure S4: A) Multiple linear regression model for prediction of ε_p in all coccolithophorid cultures with DIC between 1.6 and 3 mM. Left panel shows predicted model incorporating $CO_{2(aq)}$, growth rate, and radius, but not light. The color coding highlights a significant correlation between residuals and light. B) Same dataset, but multiple linear regression model includes light as a fourth parameter in the regression dataset.

Figure S5: A) Deviation between measured ε_p and the ε_p calculated using size and CO_2 dependencies for Western Tropical Atlantic site (ODP 925). This deviation may be due to the net effect of light and growth rate on ε_p. Also shown is the abundance of lower photic zone coccolithophores *F. profunda*, adapted for low light conditions in the deeper water column. B) Correlation between the abundance of *F. profunda* with the ε_p deviation for the Western Tropical Atlantic (ODP 925, yellow circles) and the Equatorial Pacific cores (MANOP C, blue circles). Filled circles show deviation when size-effects are accounted for, and open circles show deviation for all data assuming constant cell size.

Figure S6. Left panel shows the deviation between measured $_p$ and the $_p$ calculated using the diffusive model with constant PO_4 as in Figure 1, plotted vs CO_2 aq, for each of the four locations. Right panel shows the deviation between measured ep and the ep calculated using the statistical model as shown in FIgure 8, plotted vs CO_2 aq.

Table S1: Data from glacial –interglacial cycles including published data, new growth rate indicators, parameters and results for diffusive model ε_p calculations, and parameters and results for statistical model ε_p calculations.

Table S2: Simple correlation of culture and growth parameters with Pvar, for all cultures listed in Table 1 with ε_p determinations. All correlation coefficients indicated with * are significant ($p<0.001$).

Table S3: Parameters and results for statistical model ε_p calculations for ODP 925 and 999.

Table S4: Data from ε_{cocco}-DIC for turbidostat cultures of E. huxleyi

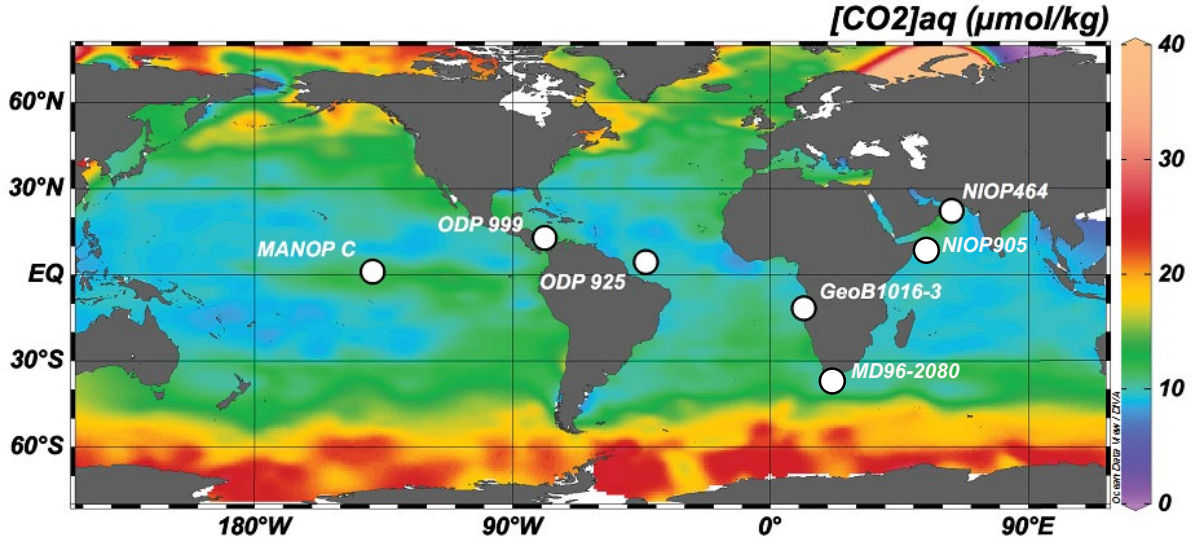
[CO2]aq (µmol/kg)
60°N
30°N
EQ
30°S
60°S
180°W
90°W
0°
90°E
40
30
20
10
0
NIOP464
NIOP905
ODP 999
MANOP C
ODP 925
GeoB1016-3
MD96-2080

Figure S1

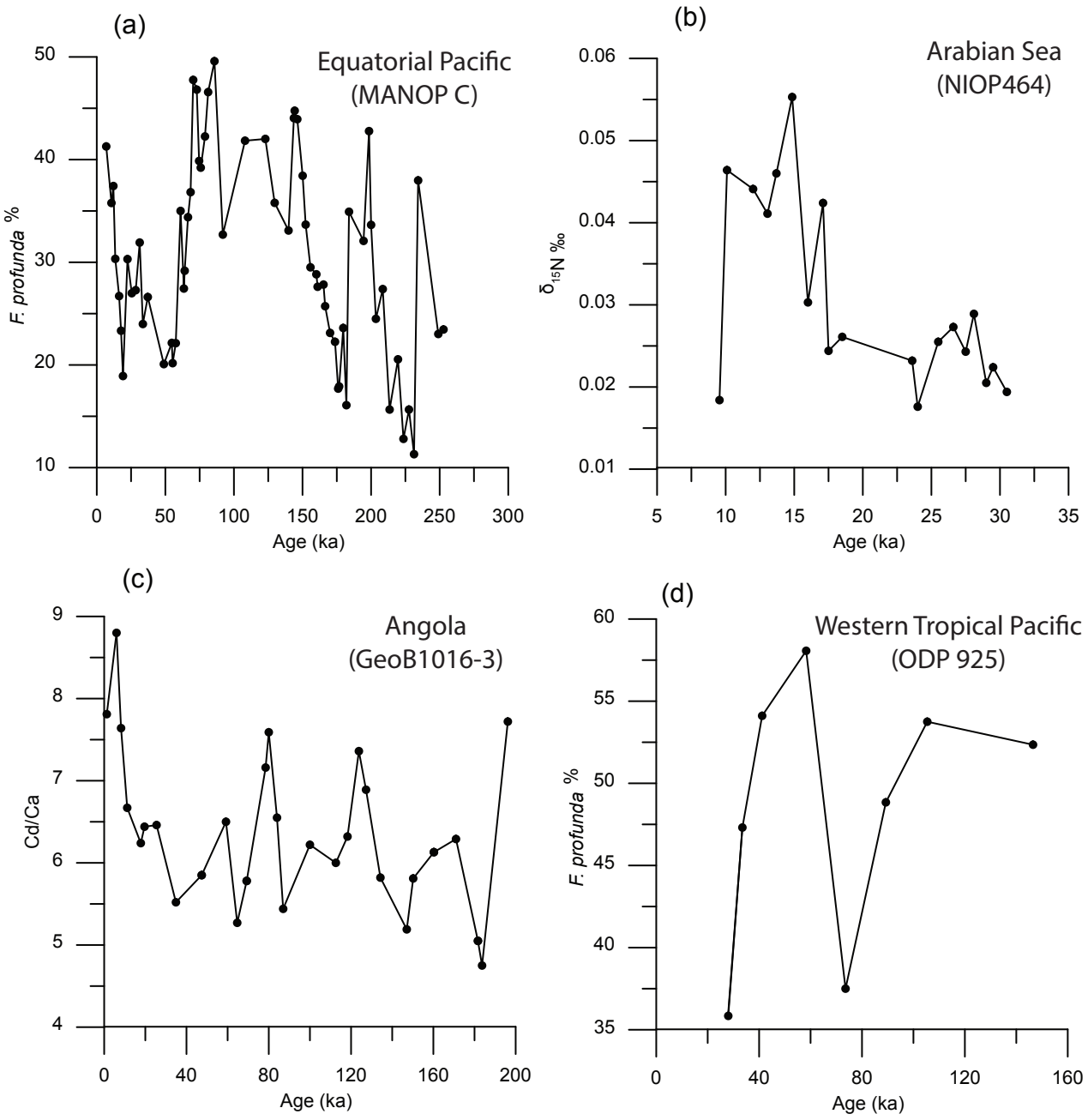
(a)
Equatorial Pacific
(MANOP C)
F. profunda %
Age (ka)
(b)
Arabian Sea
(NIOP464)
δ15N ‰
Age (ka)
(c)
Angola
(GeoB1016-3)
Cd/Ca
Age (ka)
(d)
Western Tropical Pacific
(ODP 925)
F. profunda %
Age (ka)

Figure S2

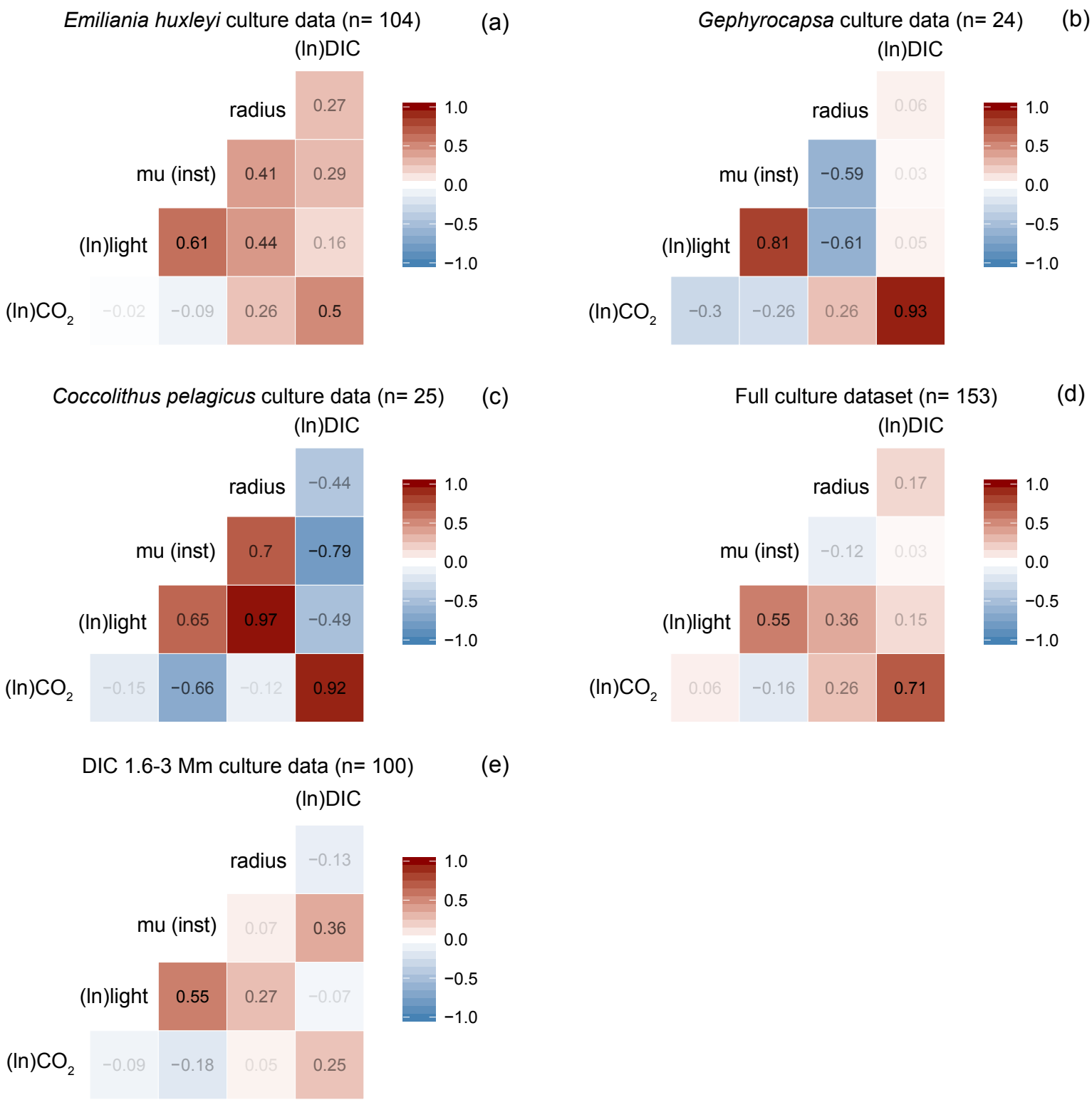
Emiliania huxleyi culture data (n= 104)
(a)
(ln)DIC
radius
mu (inst)
(ln)light
(ln)CO2
0.27
0.41
0.29
0.61
0.44
0.16
−0.02
−0.09
0.26
0.5
Gephyrocapsa culture data (n= 24)
(b)
(ln)DIC
radius
mu (inst)
(ln)light
(ln)CO2
0.06
−0.59
0.03
0.81
−0.61
0.05
−0.3
−0.26
0.26
0.93
Coccolithus pelagicus culture data (n= 25)
(c)
(ln)DIC
radius
mu (inst)
(ln)light
(ln)CO2
−0.44
0.7
−0.79
0.65
0.97
−0.49
−0.15
−0.66
−0.12
0.92
Full culture dataset (n= 153)
(d)
(ln)DIC
radius
mu (inst)
(ln)light
(ln)CO2
0.17
−0.12
0.03
0.55
0.36
0.15
0.06
−0.16
0.26
0.71
DIC 1.6-3 Mm culture data (n= 100)
(e)
(ln)DIC
radius
mu (inst)
(ln)light
(ln)CO2
−0.13
0.07
0.36
0.55
0.27
−0.07
−0.09
−0.18
0.05
0.25
1.0
0.5
0.0
−0.5
−1.0

Figure S3

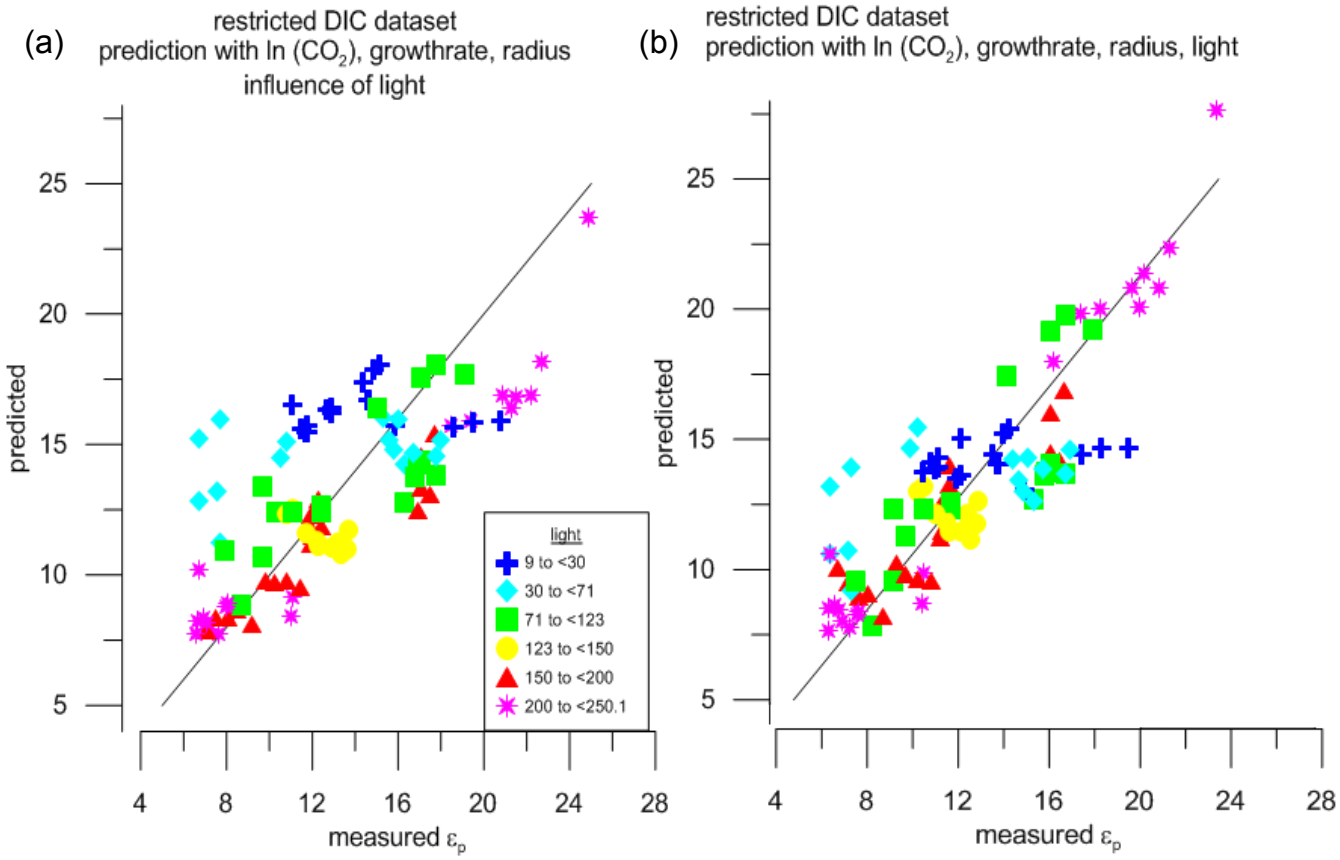
(a)
restricted DIC dataset
prediction with ln (CO_2), growthrate, radius
influence of light
(b)
restricted DIC dataset
prediction with ln (CO_2), growthrate, radius, light
predicted
measured ε_p
light
9 to <30
30 to <71
71 to <123
123 to <150
150 to <200
200 to <250.1

Figure S4

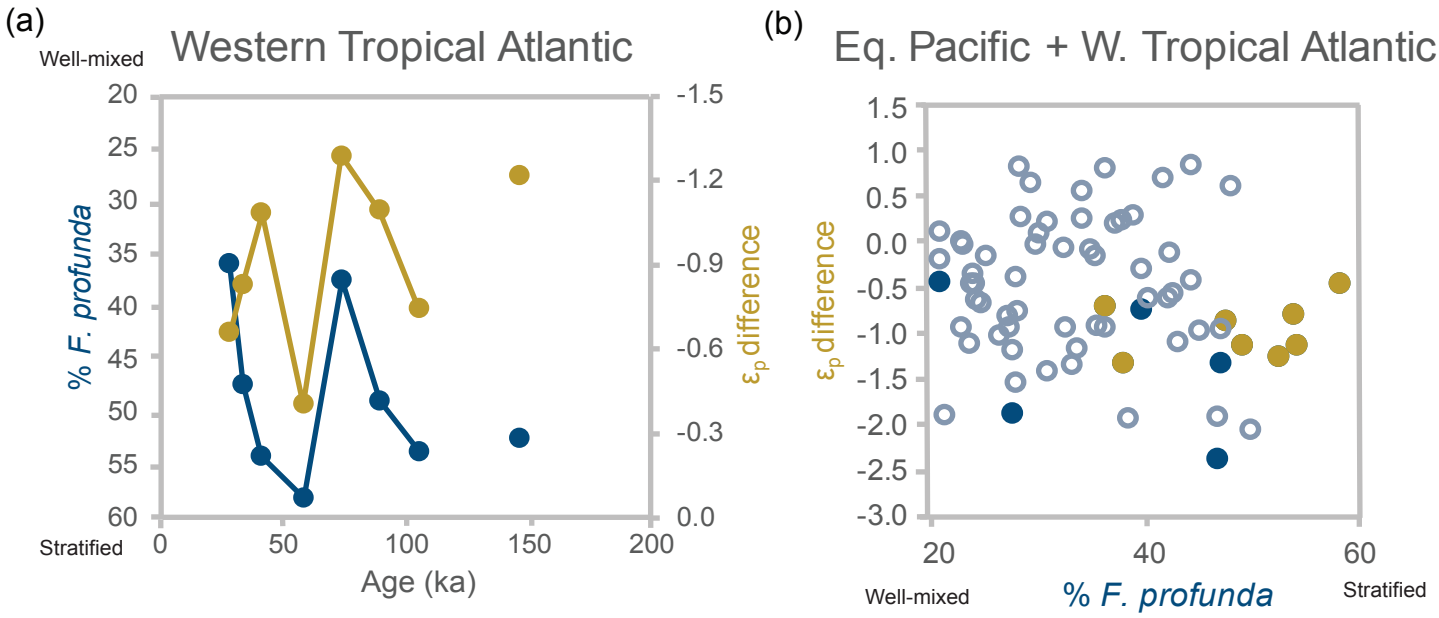
(a)
Western Tropical Atlantic
Well-mixed
Stratified
% F. profunda
Age (ka)
εp difference
(b)
Eq. Pacific + W. Tropical Atlantic
εp difference
% F. profunda
Well-mixed
Stratified

Figure S5

Figure S6

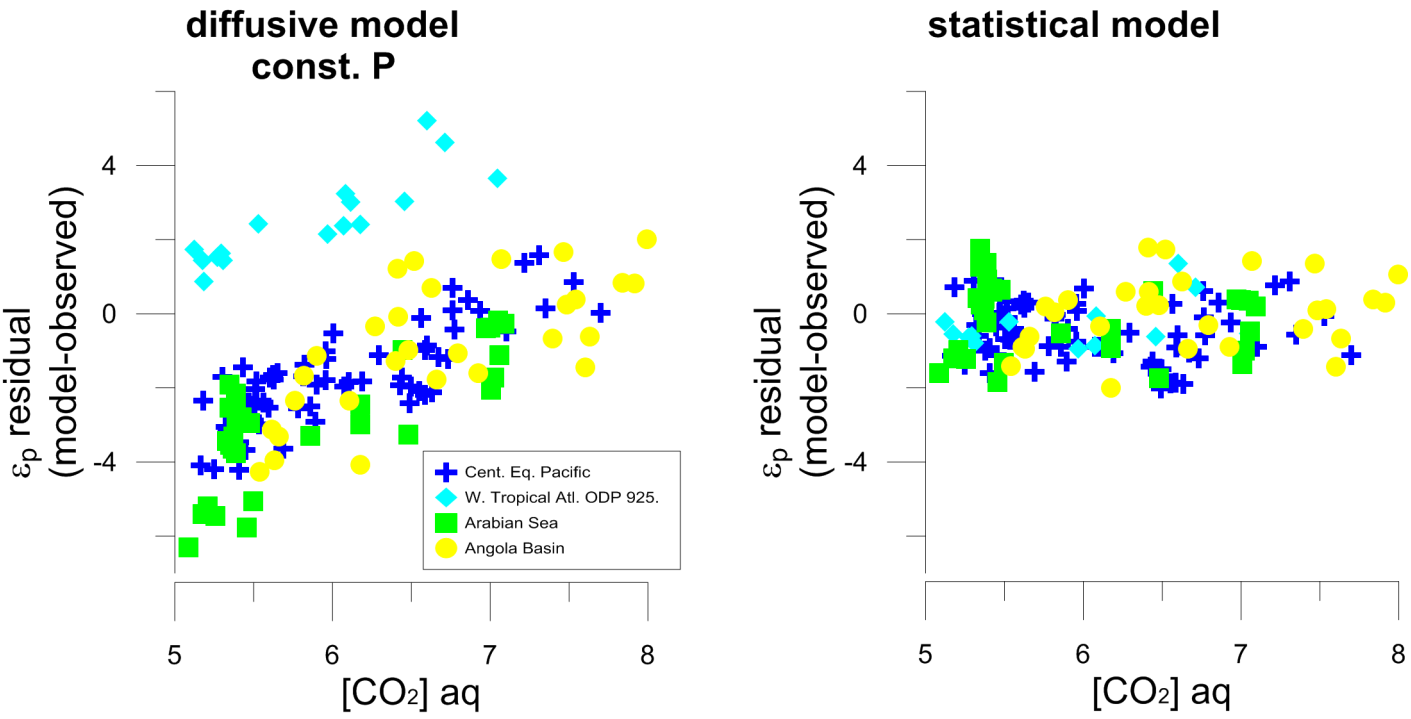
diffusive model
const. P
statistical model
εp residual
(model-observed)
4
0
-4
5
6
7
8
[CO2] aq
Cent. Eq. Pacific
W. Tropical Atl. ODP 925.
Arabian Sea
Angola Basin